REPORT DOCUMENTATION PAGE

AFRL-SR-BL-TR-00-

0509

1. AGENCY USE ONLY (Leave blank)	2. REPORT DATE	3. REPORT TYPE AND DATES COVERED
	31 August 2000	Final Report-1 June 1996 through 31 May 2000

4. TITLE AND SUBTITLE

Radiation Effects in Quantum Devices

5. FUNDING NUMBERS

(G) F49620 - 96 - 1 - 0244

6. AUTHOR(S)

Gregory F. Spencer, Wiley P. Kirk (PI),
Robert T. Bate and Richard Wilkins (Co-PI)

7. PERFORMING ORGANIZATION NAME(S) AND ADDRESS(ES)

NanoFAB Center
University of Texas at Arlington
Box 19016
Arlington, TX 76019-0016

Center for Applied Radiation Research
Prairie View A&M University
Prairie View, TX 77446

8. PERFORMING ORGANIZATION REPORT NUMBER

9. SPONSORING / MONITORING AGENCY NAME(S) AND ADDRESS(ES)

Air Force Office of Scientific Research
801 North Randolph Street, Room 732
Arlington, VA 22203-1977

10. SPONSORING / MONITORING AGENCY REPORT NUMBER

11. SUPPLEMENTARY NOTES

NONE

12a. DISTRIBUTION / AVAILABILITY STATEMENT

NO RESTRICTIONS

DISTRIBUTION STATEMENT A
Approved for Public Release
Distribution Unlimited

12b. DISTRIBUTION CODE

13. ABSTRACT *(Maximum 200 Words)*

Experiments were performed to determine the effect of radiation on quantum devices. The devices included resonant tunneling devices and two-dimensional electron gas devices. None of the devices were radiation-hardened prior to testing. The radiation used in the tests included gamma rays, protons, neutrons, and heavy ions. Resonant tunneling devices were found to possess significant radiation tolerance. None of these devices showed any systematic effects as a result of irradiation up to 1 Mrad of gamma rays, 3.5×10^{11} protons/cm^2 at 55 MeV, 5×10^{10} neutrons/cm^2 with energies from 1.5 to 800 MeV, and to 1×10^{7} Kr ions/cm^2 with an LET = 35 MeV-cm^2/mg. Two-dimensional electron gas devices, including quantum transistors and MODFET structures, were irradiated by gammas to 50 krad, protons to 5×10^{10} protons/cm^2, and neutrons to 3×10^{10} neutrons/cm^2. These devices displayed transient effects due to gamma and proton irradiation. Gamma irradiation produced a depression of the device current that recovered completely over periods of hours. Proton bombardment produced an enhancement of the device currents that did not anneal completely over similar periods. Neutron irradiation produced no effects on the devices. Taken as a whole, these results indicate that quantum devices represent a prime candidate for application in radiation-harsh environments.

14. SUBJECT TERMS	15. NUMBER OF PAGES
radiation effects, resonant tunneling devices, 2DEG, quantum devices	41
	16. PRICE CODE

17. SECURITY CLASSIFICATION OF REPORT	18. SECURITY CLASSIFICATION OF THIS PAGE	19. SECURITY CLASSIFICATION OF ABSTRACT	20. LIMITATION OF ABSTRACT
UNCLASSIFIED	UNCLASSIFIED	UNCLASSIFIED	NONE

NSN 7540-01-280-5500

Standard Form 298 (Rev. 2-89)
Prescribed by ANSI Std. Z39-18
298-102

20001016 015

RADIATION EFFECTS IN QUANTUM DEVICES

GRANT NUMBER: F49620 - 96 - 1 - 0244
STARTING DATE: 1 JUNE 1996

FINAL TECHNICAL REPORT

31 August 2000

PRINCIPLE INVESTIGATORS

Wiley P. Kirk
University of Texas at Arlington
NanoFAB Center
Box 19016
Arlington, Texas 76019-0016
817 272-2672
kirk@nanofab.tamu.edu

Thomas N. Fogarty
Center for Applied Radiation Research

Prairie View A&M University
Prairie View, Texas 77446
409 857-4606
Thomas_Fogarty@pvamu.edu

ASSOCIATES

NanoFAB Center:
Robert T. Bate
Gregory F. Spencer

CARR:
Richard Wilkins
Shojah Ardalan

Executive Summary

The primary objective of this research program was to study the effects of radiation on discrete quantum devices. Quantum devices are the fastest known electronic devices, achieving their high performance through the direct use of quantum mechanical effects such as tunneling. The quantum devices that were studied included the resonant tunneling diode (RTD) and devices based upon the two-dimensional electron gas (2DEG). The NanoFAB Center at the University of Texas at Arlington and the Center for Applied Radiation Research at Prairie View A&M University fabricated, characterized, irradiated, and analyzed a variety of quantum devices. The devices were irradiated by various sources including low and high dose gamma rays, energetic protons, high energy neutrons, and heavy ions. The radiation levels employed simulated long mission times in near-earth orbits or deep space probes into extreme radiation environments.

Experiments on individual InP-based RTDs indicated a high radiation tolerance. These devices were exposed to all of the sources listed. None of the tested devices showed any systematic changes which could be ascribed to the radiation. The exposure levels went up to 1 Mrad of ^{60}Co gamma rays, protons to a fluence of 3.5×10^{11} protons/cm^2 at 55 MeV, neutrons to 5×10^{10} neutrons/cm^2 with energies from ~1.5 to 800 MeV, and energetic heavy ions (e.g. Kr ions at 25 MeV/nucleon with LETs up to 35 MeV-cm^2/mg) on discrete RTDs. No reproducible total dose or dose rate effects were observed in the devices. This high tolerance makes RTDs a prime candidate for use in space and other radiation-hostile applications.

Experiments were also performed on GaAs-based 2DEG quantum transistors and MODFET structures. The quantum transistors displayed transient I-V changes in both 50 Krad of ^{60}Co gammas and in protons (5×10^{10} protons/cm^2 at 55MeV). Proton exposure produced an *enhanced* 2DEG channel current while exposure to gamma rays produced a 2DEG current *depression*. Both of these effects were transient with recovery periods of a few hours. Gamma-irradiated devices fully recovered to pre-radiation performance over a four hour period. Devices exposed to the protons recovered only about halfway back over the same period. The magnitude of these current transients ranged from ~40% in one heterostructure design to less than 10% variation in another. Individual MODFETs behaved in a similar manner. These devices were also exposed to neutrons to a fluence of 3×10^{10} neutrons/cm^2 with no effects on device operation. These early results in unhardened quantum devices appeared very promising for the use of these devices in radiation-harsh applications.

Objectives

The primary objective of this program was to study the effects of radiation on discrete quantum devices of several types.

New projections for faster data transmission, greater bandwidth, and higher performance will place enormous demands on future avionics and satellite electronics systems. Many of these systems will require operation at high altitudes or in near-earth orbits where harsh radiation environments exist. Additionally, the national defense infrastructure will have similar performance and survivability requirements for surveillance, data gathering, and communication systems in radiation environments that potentially far exceed the level ordinarily encountered in space. As high-altitude avionics, satellites, space probes and defense systems are given these missions of greater complexity and urgency, there is a constantly increasing need for higher performance in their electronics. The push is toward greater computational and data-manipulation power (*e.g.* ADC and DSP) and enhanced functionality in a significantly faster, more compact, and low power consuming package. The **quantum device** is one class of electronic devices that fulfills these needs. These devices work through direct quantum mechanical action based upon the precise design of the III-V semiconductor epitaxial layers and substrate and also the subsequent device fabrication. Quantum devices and integrated circuits composed of them show significant performance improvements over even advanced silicon CMOS circuits.[1] A few of these advantages are detailed in Table 1. References are also provided to the published work of others that support these conclusions.

Performance Metric	Enabling Quantum Device Characteristic	Potential Improvement over Conventional Silicon Technology	References to Others
Size & Weight	Functional compression Very high device density	Decrease of device area > 2× Reduced device count per function ~ 2 – 10×	2, 3
Power Consumption	Operation via quantum effects Reduced component count	Reduced power ~ 2 – 20× (depending on device)	3, 4
Data Manipulation Power	Very high speed Very high density	Operation to 10^{12} Hz speeds Decreased power × delay ~ 2 – 20×	5, 6

Table 1. Some possible improvements in spaceborne electronic systems that incorporate III-V quantum devices into their architecture.

In addition to these performance advantages, III-V devices, as a class, are inherently quite radiation tolerant in comparison to Si devices. When subjected to displacement damage, damage

thresholds in conventional GaAs logic and microwave devices are at least equal to Si MOS devices and superior to most Si logic devices. And field effect transistors in GaAs are relatively insensitive to total ionizing dose effects (due to x-rays, gamma rays, electrons and protons). This renders them significantly more tolerant than Si MOS devices to this radiation.

This combination, large performance improvements over conventional circuits and materials with an enhanced radiation tolerance, suggests that III-V quantum devices are an important, untapped resource for space applications.

Summary of Effort

This research project was a collaboration between the Center for Nanostructure Materials and Quantum Device Fabrication (the NanoFAB Center) of the University of Texas at Arlington in Arlington, Texas, and the Center for Applied Radiation Research of Prairie View A&M University in Prairie View, Texas. These two groups brought their respective strengths together to perform the wide range of required tasks.

The NanoFAB Center fabricated quantum devices for irradiation by PVAMU CARR and provided for initial baseline characterization of all the devices obtained for the project. Large-area two-dimensional electron gas (2DEG) devices were fabricated using the Center's III-V MBE system to provide GaAs/AlGaAs-based substrates. Other devices obtained by NanoFAB include in-plane gated 2DEG transistors (IPGT) made by focused ion lithography from the Ruhr Universität Bochum in Germany (headed by Prof. Andreas Wieck) and InGaAs/InP-based RTDs from Raytheon-TI Systems. All the devices provided to CARR were characterized at room temperature and, where appropriate, at low temperatures to determine their initial baseline behavior.

PVAMU CARR performed radiation testing of these devices. Testing of RTDs and 2DEG devices under a variety of radiation sources was performed. These radiation sources included ^{60}Co gamma rays, protons, neutrons, and heavy ions at the facilities listed in Table 4 (see page 10). Both CARR and NanoFAB participated in the analysis of the test data.

In this section, a review is presented of the discrete devices that were radiation tested. Next, a summary of the important results of the project is given. This is followed by recommendations for future work to enable the use of quantum devices in space applications.

Devices Tested

In the course of this project, a variety of discrete quantum devices were fabricated and radiation tested. All of the devices were built on epitaxial heterostructure substrates of the Group III-V compound semiconductors. These included heterostructures comprising both two-dimensional electron gas behavior and resonant tunneling behavior. The compositions and properties of the 2DEG heterostructures are presented in Table 2.

Layer \ Substrate	NanoFAB H039	Raytheon 5793	RU 9351	RU 1216
n GaAs cap	50 nm ~2×10^{18} cm^{-3}	50 nm 2×10^{18} cm^{-3}	5.5 nm undoped	~5 nm 5×10^{15} cm^{-3}
n $Al_xGa_{1-x}As$ donor	30 nm x = 0.25 2×10^{18} cm^{-3}	30 nm x = 0.25 2×10^{18} cm^{-3}	72 nm x = 0.21 2×10^{18} cm^{-3}	x = 0.3 3×10^{18} cm^{-3}
Undoped AlGaAs spacer	10 nm	20 nm	2.7 nm	5.7 nm
Undoped GaAs buffer	1.06 μm	1 μm	11.3 nm $In_{0.1}Ga_{0.9}As$ channel on 930 nm GaAs	8.1 nm $In_{0.25}Ga_{0.75}As$ channel on 650 nm GaAs
Getter layer	none	none	superlattice with 30 periods of 3 nm AlGaAs & 3 nm GaAs, 1 μm GaAs buffer	superlattice with 10 periods of 9.9 nm AlGaAs & 5.1 nm GaAs on 1 μm GaAs buffer
Semi-insulating GaAs substrate	SI GaAs	SI GaAs	SI GaAs	SI GaAs
Mobility at low temperature	1×10^{5} cm^2/Vs (77 K)	2.7×10^{5} cm^2/Vs (4.2 K)	4.69×10^{4} cm^2/Vs (77 K)	3.18×10^{4} cm^2/Vs (4.2 K)
Carrier density at low temperature	5×10^{11} cm^{-2} (77 K)	6.85×10^{11} cm^{-2} (4.2 K)	1.2×10^{12} cm^{-2} (77 K)	1.14×10^{12} cm^{-2} (4.2 K)

Table 2. Some of the standard 2DEG epitaxial layers used for device fabrication and some of their physical properties prior to radiation testing.

At the NanoFAB Center, two-dimensional electron gas devices were fabricated in the GaAs/AlGaAs materials system. First, 2DEG heterostructures were grown using the Center's advanced MBE facility. The details of the primary substrate were presented in Table 2. The 2DEG devices fabricated on substrate H039 included large-area Hall bars and ungated MODFETs with characteristic channel widths ranging from 100 μm down to 6 μm and channel lengths from 100 μm to 3 μm. These devices were fabricated by standard photolithography, lift-off metallization and annealing, and mesa isolation by wet chemical etch. Some of the devices in the chip layout are shown in the SEM micrograph of Figure 1. Use of the Hall bar configuration permitted standard magnetotransport measurements to characterize important substrate properties as well as providing device structures for irradiation.

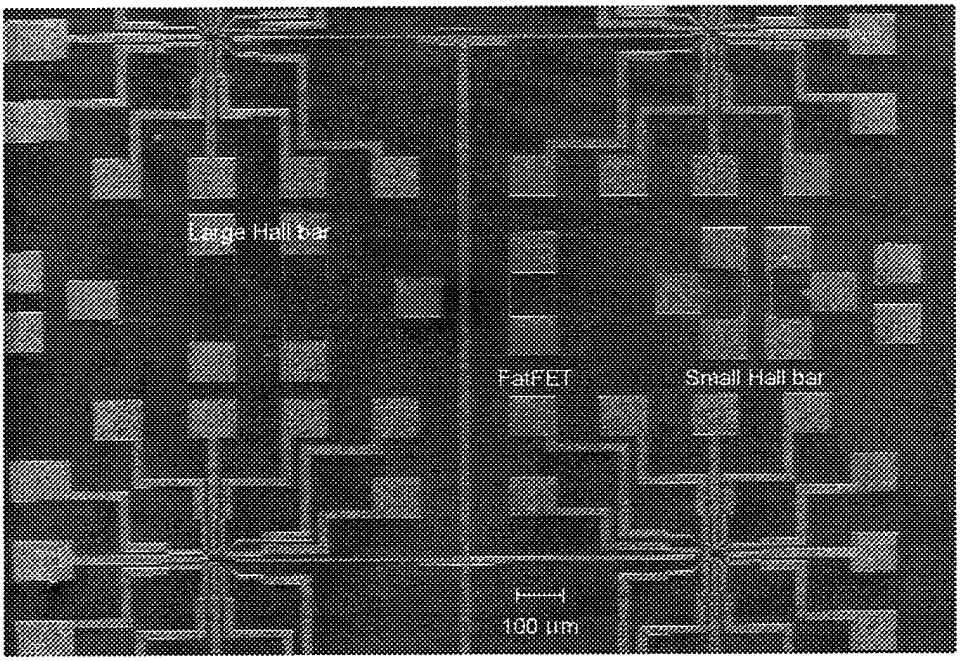

Figure 1. SEM micrograph of some of the large-area devices fabricated on NanoFAB Center GaAs/AlGaAs heterostructures. The large Hall bar has a channel width of 100 μm and a SD length of 600 μm. The small Hall bar has a width of 10 μm and a SD length of 200 μm.

Three-terminal 2DEG devices were obtained from our collaborators at the Ruhr Universität Bochum in Germany. These transistor-like devices were fabricated in a manner similar to the NanoFAB devices. In this case, final device definition was achieved by using focused ion beam lithography (FIB). The critical difference between these devices and an ordinary transistor was in the nature of the gates. Rather than employ a metal/semiconductor top-gate as in simple MOSFETs or an intervening region of opposing carriers as in BJTs, these

devices utilized the 2DEG as both the conduction channel and the gates. After mesa isolation created the circular 2DEG mesa, seen in Figure 2, the FIB step isolated regions on the mesa from one another. These electrically isolated regions could then act as both source-drain for current flow and as in-plane gates for switching. The devices were typically fabricated for operation in depletion mode. The in-plane gated transistors (IPGT) were fabricated on two slightly different substrates (RU9351 and RU1216).

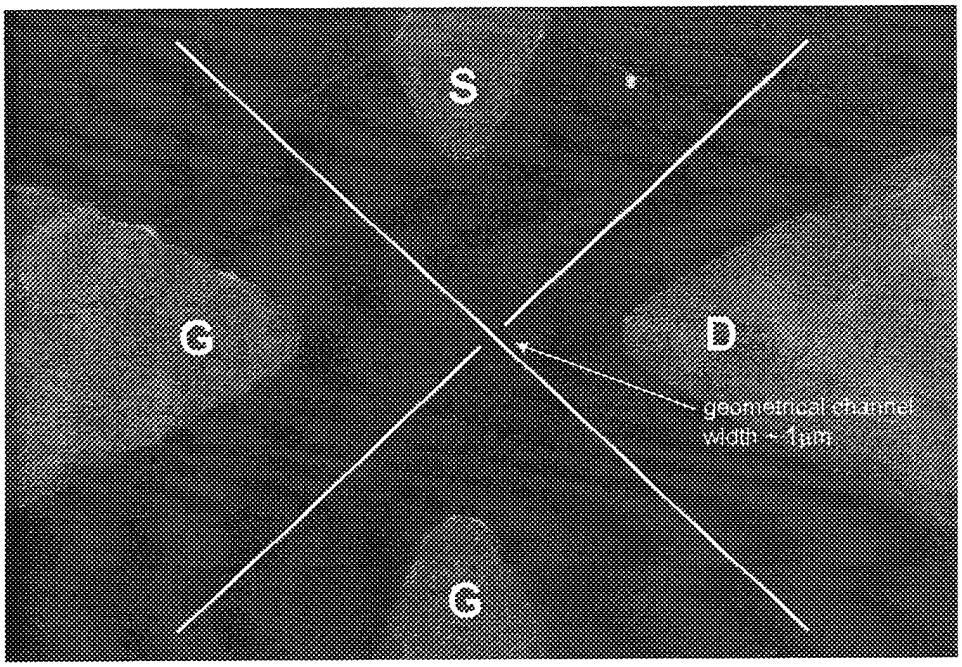

Figure 2. SEM micrograph of the active region of a 2DEG in-plane gated transistor fabricated at Ruhr Universität Bochum. The white lines have been added to indicate the focused ion beam tracks which patterned the circular 2DEG mesa into electrically isolated regions to form the three-terminal device.

Resonant tunneling devices (RTDs), fabricated on InP substrates at Raytheon, were also characterized and radiation tested. These materials utilize lattice-matched InGaAs quantum wells surrounded by AlAs tunnel barriers as well as the possibility of narrow bandgap InAs layers to better control and tune the available tunneling states. This material system offers a significant advantage by allowing quantum behavior to appear at room temperatures (for example, see Figure 5 for IV data at 300K). The design of the tunneling region of the epitaxial substrate is in given in Table 3 and the band structure in the double barrier region is shown in Figure 3. These devices were built in a number of different two and three-terminal configurations. Shown in the SEM micrograph of Figure 4 is one style of three-terminal device that was irradiated.

Layer	Material
Undoped spacer layer	2.0 nm $In_xGa_{1-x}As$
Tunnel barrier	2.3 nm AlAs
Quantum well	1.0 nm $In_xGa_{1-x}As$, x=0.53
Narrow bandgap notch	2.0 nm InAs
Quantum well	1.0 nm $In_xGa_{1-x}As$, x=0.53
Tunnel barrier	2.3 nm AlAs
Undoped spacer layer	2.0 nm $In_xGa_{1-x}As$

Table 3. Design of one of the epitaxial substrates used for making resonant tunneling devices, which display quantum behavior at room temperature.

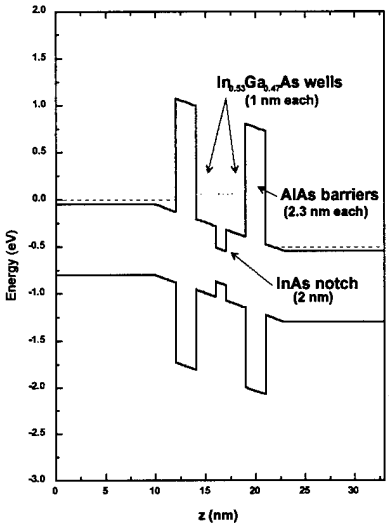

Figure 3. Band diagram of the RTD substrate provided by Raytheon-TI Systems in the quantum well region.

This tunneling structure (based on their growth sample #202-2138) consisted of double barriers of AlAs (each 2.3 nm thick) surrounding two lattice-matched quantum wells of $In_{0.53}Ga_{0.47}As$ (1 nm each) separated by an InAs notch in the middle (2 nm thick). Undoped spacer layers of lattice-matched InGaAs (2 nm) were grown on both sides of this double-barrier structure and the epilayers were grown with standard cap and buffer layers on an Fe-doped InP substrate.

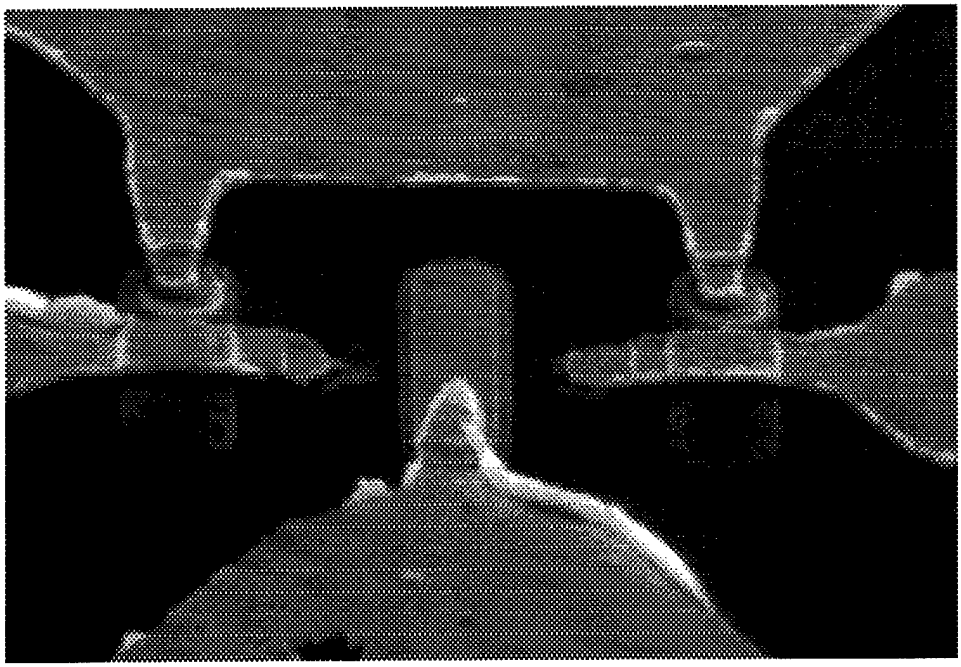

Figure 4. SEM micrograph of an InP-based RTD built into a three-terminal configuration.

Radiation Sources

A wide variety of radiation sources were employed for testing of the devices. The different kinds of radiation included ^{60}Co gamma rays, energetic protons and neutrons, and heavy ions. The devices were tested to look for total dose effects. Although devices were exposed to various radiation sources at different dose rates, no systematic dose rate studies were performed. In each case, the total dose applied to the test devices was chosen to represent either a significant mission period in a near-earth orbit, corresponding to mission times of 5 to 10 years, or a mission into an extreme radiation environment such as the vicinity of Jupiter or its moon Io. Devices were irradiated in the facilities presented in Table 4.

Radiation Type	**Facility**
^{60}Co gamma	a. Texas A&M Veterinary School b. Prairie View A&M University c. University of Houston (high dose)
protons	Texas A&M Cyclotron Institute
neutrons	Los Alamos Neutron Science Center
heavy ions	Texas A&M Cyclotron Institute

Table 4. List of radiation facilities employed in these experiments.

Summary of Radiation Test Results

The quantum devices showed radiation tolerances that ranged from near immunity at the levels tested to exhibiting small-to-moderate transient changes due to irradiation. These data were the first to indicate that some quantum devices possessed radiation tolerances sufficient to make them excellent candidates for space applications. The differing device tolerances fell along device type. Devices that employed depletion barriers were more susceptible to radiation-induced changes. Those that used band structure offsets and resonant tunneling were far less susceptible. The general results of the radiation tests are briefly discussed here.

Of greatest interest was the fact that resonant tunneling devices displayed no effects for any of the radiation sources applied against them. By the conclusion of the RTD testing, no total dose effects were observed including no changes in the device operation and even no observable transient effects. The RTDs were irradiated by up to 1 Mrad of ^{60}Co gamma rays, energetic protons (55 MeV) to 3.5×10^{11} p^+/cm^2, a neutron spectrum (1.5 to 800 MeV) to 5×10^{10} n^0/cm^2, and heavy ions (Kr with LET = 19 and 35 MeV/mg/cm^2) to 1×10^7 particles/cm^2. In each case, the post-irradiation data displayed no systematic changes from the pre-irradiation data.

The results from the 2DEG devices were more complex. These devices, both large area and small, did exhibit operational changes due to irradiation by ionizing radiation and charged particles. Bombardment by neutral particles, neutrons, resulted in no changes. Changes in devices channel currents were observed which depended upon both the device substrate layers and also the type of radiation. These devices were irradiated by ^{60}Co gamma rays up to a maximum of 50-65 krad total dose and also 55 MeV protons to 5×10^{10} p^+/cm^2. Either of these sources produced transient changes in the channel current. Gamma irradiation produced a reduction in current while proton irradiation produced an enhancement of the current. The gamma transients relaxed back to pre-radiation current values within about 4 hours of the irradiation. Over similar time periods the proton transients relaxed only about halfway back to the pre-radiation level. The size of the transients appeared to depend upon the substrate details with the effects ranging from ~40% initially down to 6% changes on later substrates. However, exposure to 3×10^{10} neutrons/cm^2 produced no observable changes in these devices.

Conclusions and Suggestions for Further Study

A primary conclusion from this project was that the InP-based resonant tunneling devices were an excellent candidate for space or other radiation-harsh applications. Up to the highest levels of irradiation reached, the RTDs displayed no changes from their pre-radiation behavior. The devices tested were not radiation-hardened in any way, but were tested as fabricated. Similar RTDs have been irradiated to much higher proton fluences (7×10^{14} cm^{-2} at 3 MeV) and have shown systematic radiation effects.[7]

Two-dimensional electron gas devices did show transient radiation effects due to exposure to either energetic charged particles (protons) or to ionizing radiation (gamma rays). The magnitude of the transients seemed to depend upon substrate. This indicated that optimization of the substrate and device design might increase the radiation tolerance of these devices against exposure to protons and gamma rays. On the other hand, these devices displayed no changes due to bombardment by energetic neutrons.

Since the thrust of the current research was centered upon discrete quantum devices, a natural next step would be to fabricate these devices into functional integrated circuits. Such quantum ICs would possess the full operational advantages of the individual devices. Radiation testing of these ICs would seek to determine whether the circuits retain the radiation hardiness of the discrete devices. If so, then quantum integrated circuits would become an important component of high performance electronics suitable for radiation-harsh environments.

Accomplishments and New Findings

Radiation Testing Procedure

The following procedure was used throughout the experiments. A pre-radiation measurement was performed on the device once it had been mounted in the test fixture. Subsequently, the device was incrementally exposed to the radiation source and remeasured after each increment. Finally, if changes had been observed in its behavior during irradiation, then the device was followed for a period of time after the completion of the exposure to look for signs of recovery.

Resonant Tunneling Devices

Pre-Radiation Characterization

Prior to any irradiation studies, baseline transport measurements on the quantum devices were made at the NanoFAB Center. Initial room- and low-temperature I-V and magnetotransport measurements were performed on the resonant tunnel diodes obtained from Raytheon. Room-temperature I-V measurements were done with the sample packages mounted in a breadboard. The RTD was connected to a DC voltage source in series with a 10 Ω current-sense resistor. Voltmeters (HP 3478A DVM) recorded the voltages across the current-sense resistor and across the device, and the voltage source was swept slowly under computer control in 10 mV steps between ±2V starting at 0V. To suppress circuit oscillations, especially in the region of negative differential resistance (NDR), a 10 nF capacitor was connected in parallel with the RTD.[8,9]

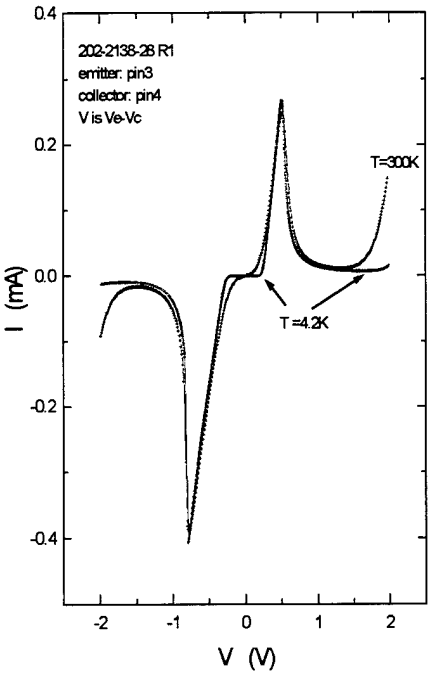

Figure 5. I-V characteristics of sample 202-2138-28 R1. I-V curves taken for both room-temperature (300K) and low temperature (4.2K) are shown.

Low-temperature (4.2 K) measurements were done with the device mounted in a sample probe, immersed in a liquid helium cryostat. A small-area device was used, with a $2\times2\mu m^2$ cross-section perpendicular to the current flow, to minimize device current and heat dissipation,

as well as to avoid the step-like features often seen in the I-V curves which are associated with device or circuit oscillations in the NDR region. Both room- and low-temperature I-V curves are shown for this device in Figure 5. The curves are remarkably similar, differing principally by the sharper turn-on characteristics of the current at low temperature, as well as a wider valley region at 4.2 K.

Once the devices had been readied for irradiation, the baseline measurements were repeated in the PVAMU setup. One such pre-radiation result for an RTD is shown in Figure 6. The structure in the NDR region was due to details of the external circuit that had different filtering from the initial tests. The observed oscillations were typical of devices that display NDR and did not affect the results.

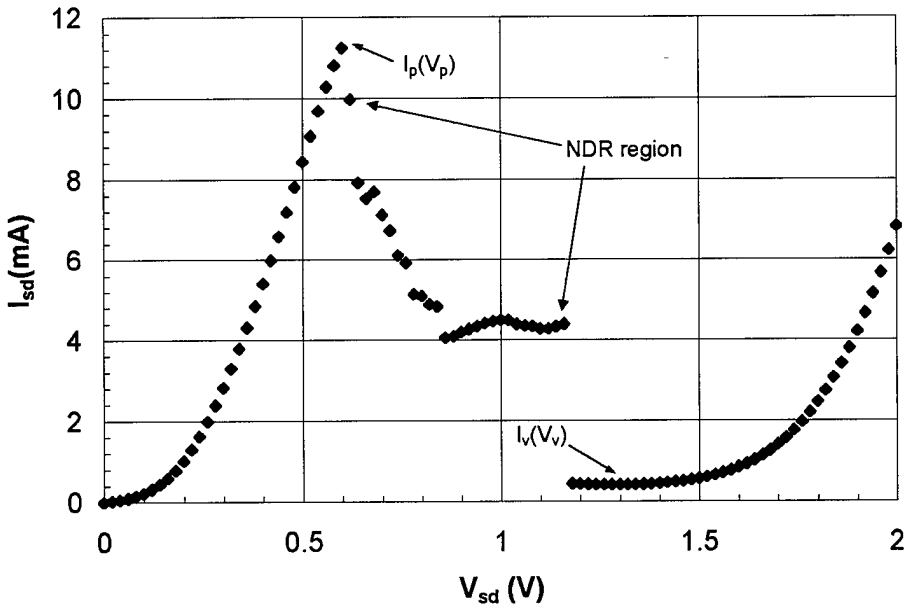

Figure 6. IV characteristic of an RTD prior to irradiation. Important features of the curve are labeled. The structure seen in the NDR region is due to external circuit details.

One of the primary figures of merit for an RTD is the ratio of its peak current, $I_p(V_p)$, to its minimum valley current, $I_v(V_v)$. These two currents are indicated in Figure 6. This peak-to-valley current ratio, PVR = I_p/I_v, is a sensitive indicator of the electronic tunneling through the double-barrier heterostructure. The PVR for the InP-based RTDs in this study was in the range of 25-30 at room temperature, rising to 40 at cryogenic temperatures.

Gamma Irradiation

RTDs were exposed to gamma radiation from a ^{60}Co source at the Texas A&M Veterinary School. The InP-based RTDs were found to be quite radiation tolerant up to the maximum radiation exposures applied. No definitive, systematic radiation effect was seen on the peak-to-valley current ratio (I_p/I_v) for any of the tested devices.

Initial tests using gamma radiation (^{60}Co source) to total doses of 50 Krad, at a dose rate of about 50 rad/min, showed no systematic effects on (I_p/I_v). In addition there were no observed voltage shifts of I_p. The initial tests were conducted measuring the current-voltage (I-V) characteristics of the devices by ex-situ techniques after irradiation. Subsequent tests were conducted in-situ with the I-V characteristics being measured during irradiation. These later measurements were also done to a total dose of 50 Krad at a higher dose rate of about 255 rad/min. Results from one of the RTD tests are presented in Figure 7 in which both the pre-radiation and post-radiation data are plotted. At the level of exposure for this device, 51 Krad, no effects of irradiation were seen. The pre- and post-exposure curves appeared nearly identical in these tests.

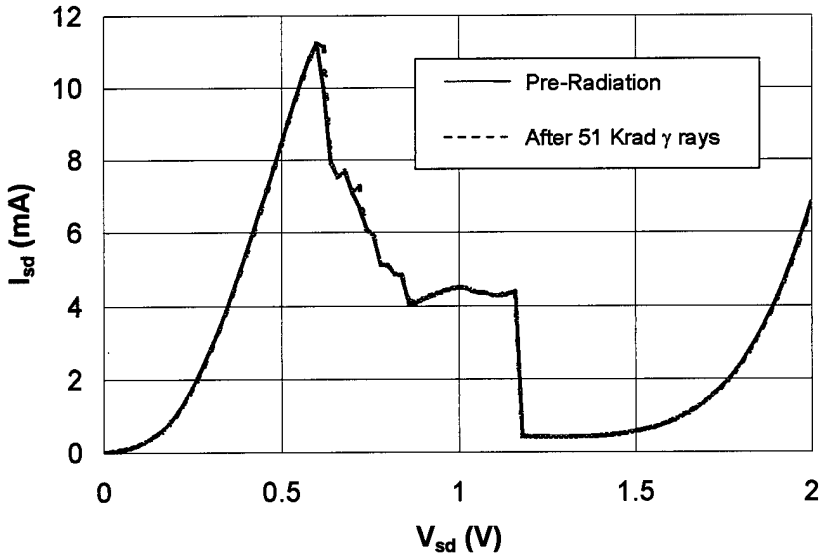

Figure 7. I-V characteristics of an RTD before and after exposure to 51 krad of ^{60}Co γ rays.

In order to make a closer inspection of the RTD/gamma data, the pre-radiation I-V curve was subtracted from the post-radiation curve, and the difference normalized by the peak current, I_p. If the two curves were identical in shape and had no unaccounted voltage shift or other

differences, then a flat line would be the result. The actual result, $\delta I/I_p = [I(post) - I(pre)]/I_p$, is presented in Figure 8 and compares the I-V data before and after 51 krad of ^{60}Co gamma rays. The residual curvature, with a magnitude less than 0.5% of I_p, in the solid data points resulted from an unidentified, small voltage shift in the I-V curve. For comparison, the open data points of Figure 8 were obtained by shifting of the pre-radiation curve by +2 mV and then subtracting the shifted curve from the original. The two resulting curves, the real data comparison and generated curve, are almost coincident. The sign of the curvature, $\delta I/I_p$, depended upon the sign of the voltage shift. Shifts of this size were observed for unirradiated devices as well and therefore were not ascribed to radiation effects. This comparison put a further limit on the magnitude of radiation effects to only a few tenths of one percent. Small changes in peak and valley minimum currents, $I(V_p)$ and $I(V_v)$, were observed which resulted in a decrease of the RTD PVR by about 2% after irradiation. Similar results were seen with other radiation sources.

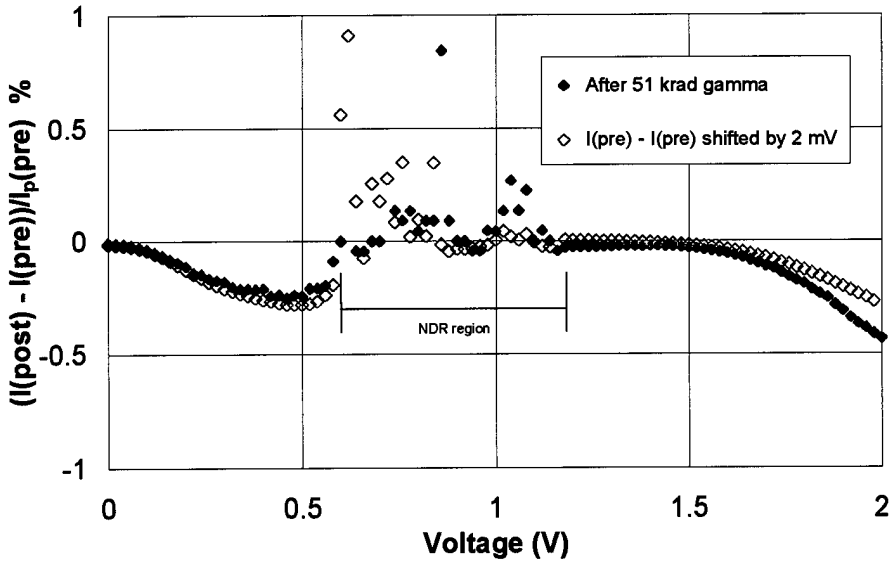

Figure 8. Change in the RTD current relative to I_p (solid data). The two I-V curves, pre- and post-exposure, were the same to within a few tenths of a percent. The open points were obtained by shifting the unirradiated I-V curve by +2 mV and subtracting this from itself.

To study the gamma susceptibility further, RTDs were exposed to a high dose gamma source at the University of Houston. The total dose was 1 Mrad at a rate of 175 krad/hour. This amounted to a total dose increase by a factor of 20 and a dose rate increase by a factor of almost

60. These devices still displayed no measurable effect in their IV behavior in either the baseline PVR or $V(I_p)$. This is illustrated in the data plot for one of the irradiated devices in Figure 9.

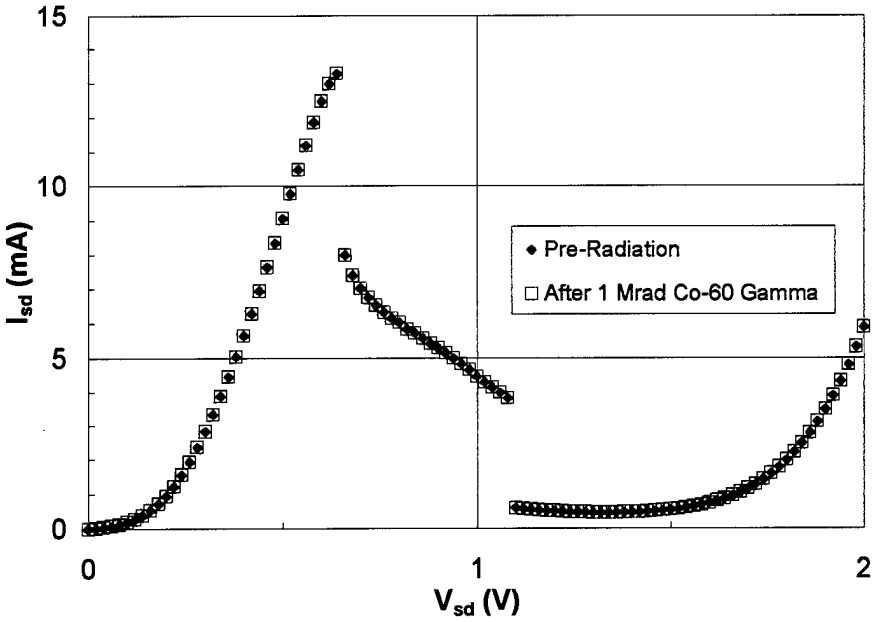

Figure 9. I-V characteristic of an RTD before and after exposure to 1 Mrad of ^{60}Co γ rays.

The variation of the PVR with gamma dose is illustrated in Figure 10. Although small variations in the magnitude of the PVR were observed, of the order of 2 percent or less, none varied systematically with total dose. Therefore these were not regarded as radiation effects. Additionally, the PVR variation for the different gamma dose rates is shown in Figure 11, once again displaying nonsystematic changes of less than 2%.

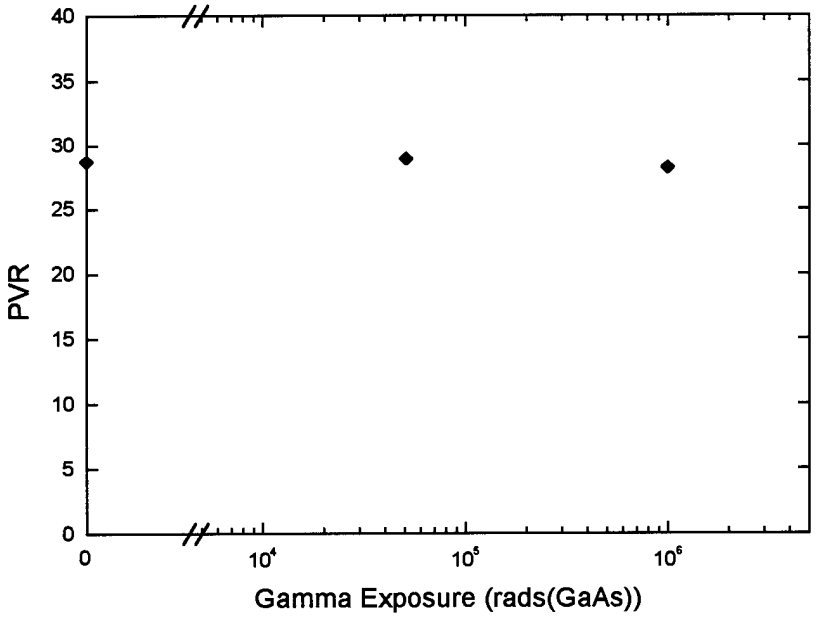

Figure 10. Variation of the peak-to-valley ratio for an RTD over the whole total dose range of the experiments.

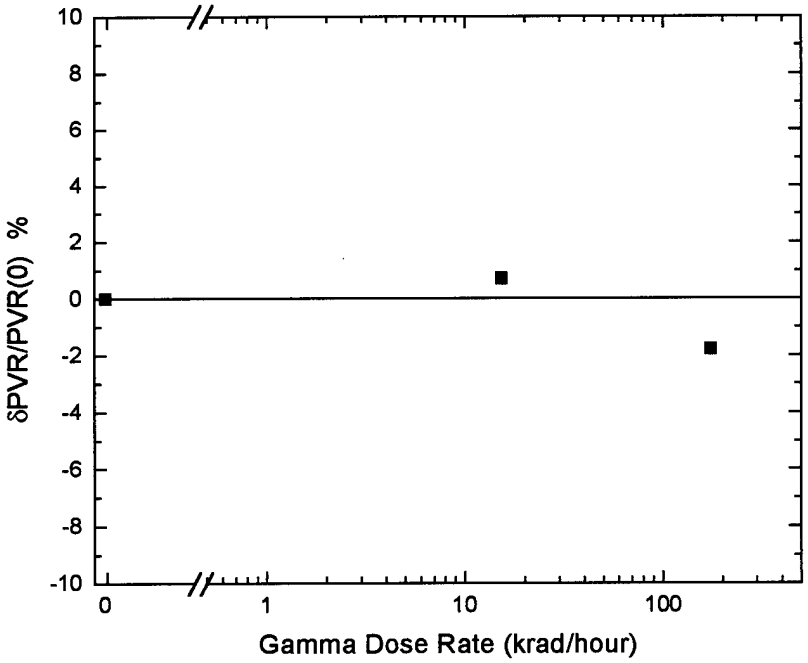

Figure 11. Variation of the PVR over the range of gamma dose rates that were employed.

Proton Irradiation

Proton tests of the RTDs were conducted at the Texas A&M Cyclotron Institute. The proton beams had an energy of 55 MeV, with a typical flux near 5×10^7 protons/cm^2-sec. In-situ measurements of the I-V characteristics were made for various values of exposure up to a total

fluence of 5×10^{10} protons/cm^2. No systematic effects were observed on the magnitude of the PVR for any of the RTDs tested. In addition, no voltage shift of the peak current I_p was observed. Some of the RTDs were irradiated to a higher total fluence of 3.5×10^{11} protons/cm^2 with no observed effects on the I-V characteristics. Data from one of the RTDs is shown in Figure 12. Once again, no significant changes can be seen in the irradiated device from low to higher exposure doses. The minor differences in the NDR region can't be ascribed to the exposure due to the sensitivity of that region to exact circuit, materials, and experimental details, as discussed earlier.

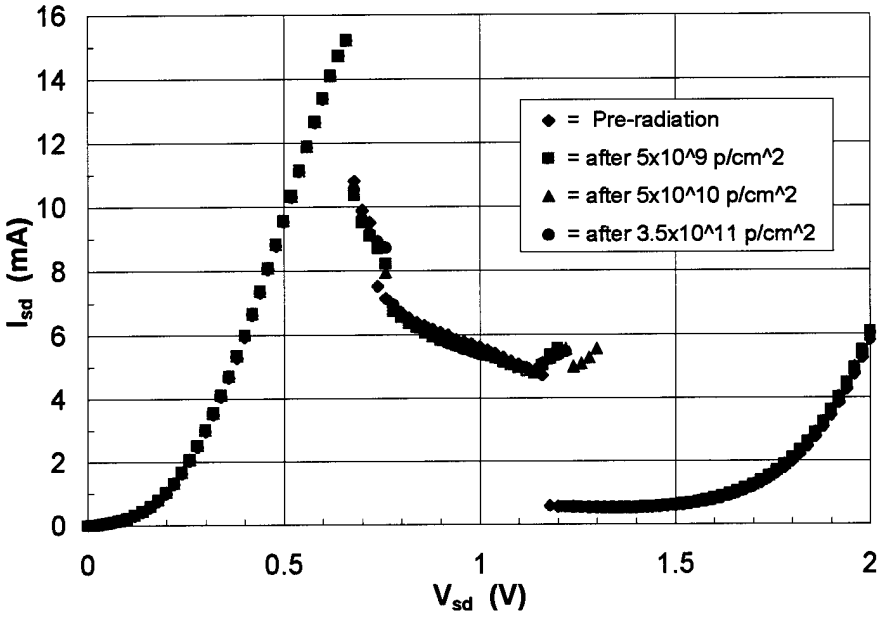

Figure 12. I-V characteristics for an RTD before and after bombardment by 55 MeV protons to fluences of 5×10^9, 5×10^{10}, and 3.5×10^{11} protons/cm^2 at a flux of 5×10^7 protons/cm^2-sec.

As with the case of the gamma irradiation, the PVR of the proton-irradiated RTDs was not found to vary systematically with the proton fluence. The overall variation of their PVR was about 1% at the highest fluence, with similar variations seen in the lower exposures. In this case, all the variations were found to be decreases in the PVR. This is shown in Figure 13.

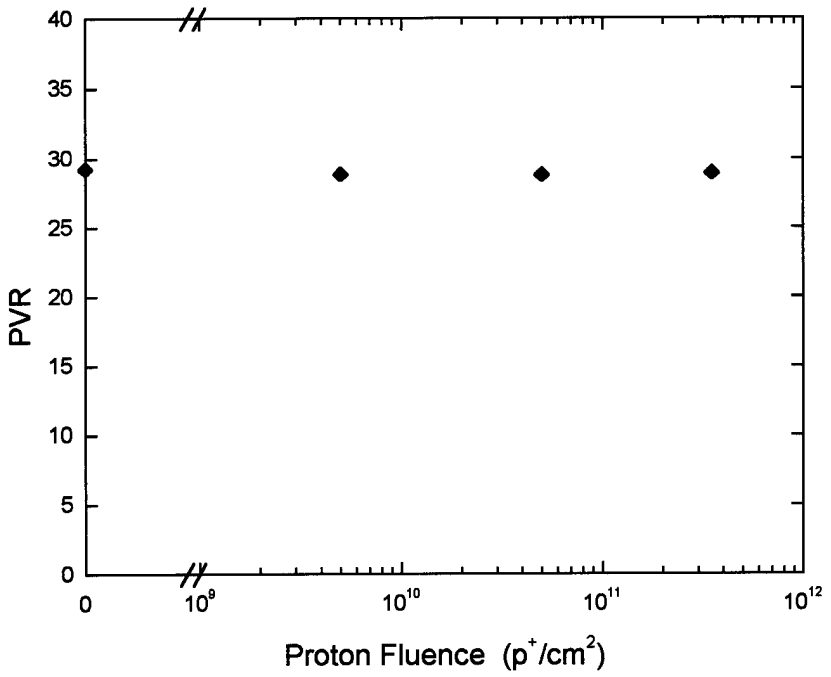

Figure 13. Variation of the peak-to-valley ratio for an RTD irradiated by 55 MeV protons up to a maximum fluence of 3.5×10^{11} protons/cm^2. The maximum variation of the PVR was about 1.5%.

The modeling efforts on RTDs focused on simulating RTD characteristics using a SILVACO quantum simulator at the University of Texas at Arlington and a NEMO quantum simulator from researchers at Raytheon-TI Systems. The method used to simulate radiation damage in the quantum wells was to apply and vary doping profiles in and around the tunnel barriers and quantum well regions of the device. This approach assumed that the proton irradiation created electrically active defects in the well which modified the tunneling characteristics. These simulation results suggested that a voltage shift for the peak current I_p would occur at high total fluences, above 10^{13} protons/cm^2. This was a higher exposure than these experiments reached at current facilities.

Neutron Irradiation

Individual RTDs were irradiated by neutrons from a high-energy ablation source. This experiment was performed at the Los Alamos Neutron Science Center. The source simulated the atmospheric neutron spectrum at an altitude of approximately 40,000 ft and produced neutrons ranging from 1–800 MeV to a fluence of 5×10^{10} neutrons/cm^2. A data set from this test is shown in Figure 14. No systematic changes were observed in the I-V characteristics of the RTDs during this experiment.

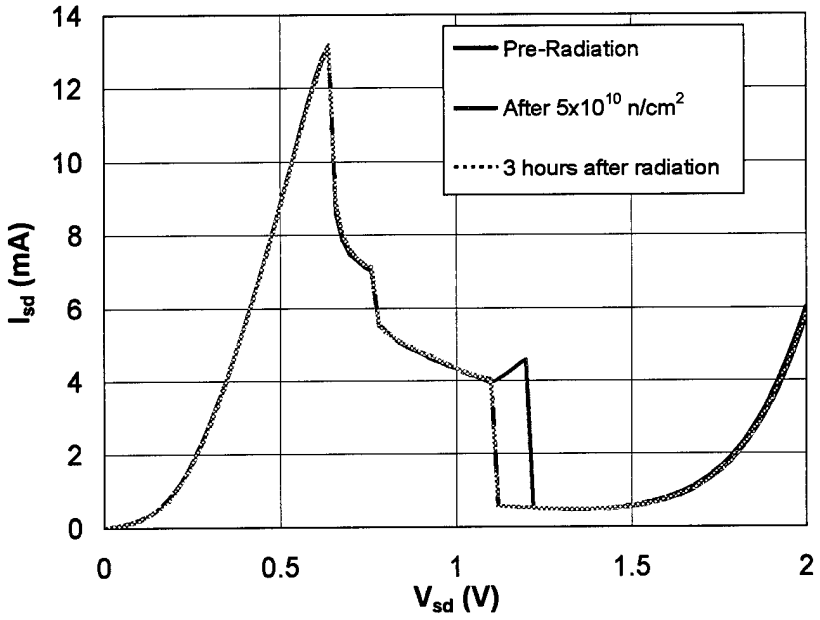

Figure 14. I-V characteristic of an RTD irradiated by energetic neutrons (up to 800 MeV). No systematic changes in the device behavior were observed.

Heavy Ion Bombardment

To determine the effects of more massive projectiles, some RTDs were irradiated by heavy ions. Irradiations were performed using Kr ions with a linear energy transfer (LET) of 19 MeV-cm^2/mg and 25 MeV/nucleon. Data from one such trial is shown in Figure 15.

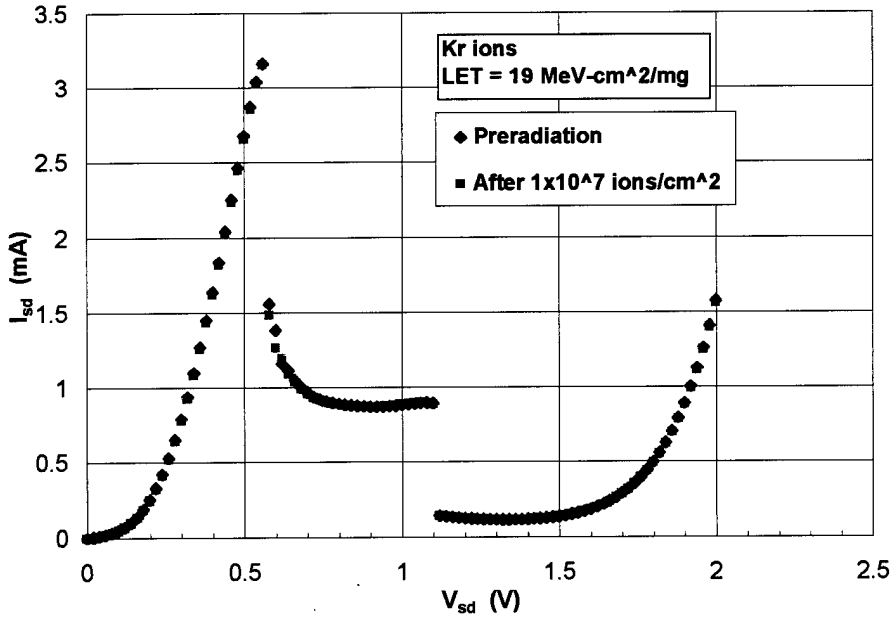

Figure 15. I-V curve of an RTD exposed to 25 MeV/nucleon Kr ions with an LET = 19 MeV-cm^2/mg to a fluence of 1×10^7 ion/cm^2.

Shown in Figure 16 are the results from Kr bombardment to an LET = 35 MeV-cm^2/mg. In addition, Ne ions with an LET of 2.5 MeV-cm^2/mg were used. The fluence for each run was 1×10^7 particles/cm^2. Again, no effects were observed on the electrical behavior of individual devices at these levels.

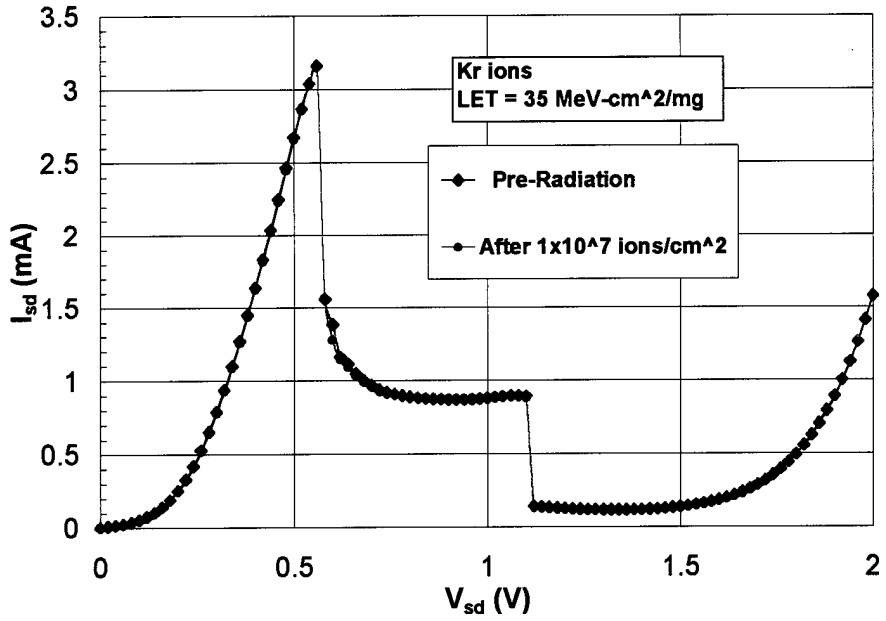

Figure 16. I-V curve of an RTD exposed to Kr ions with an LET of 35 MeV-cm^2/mg.

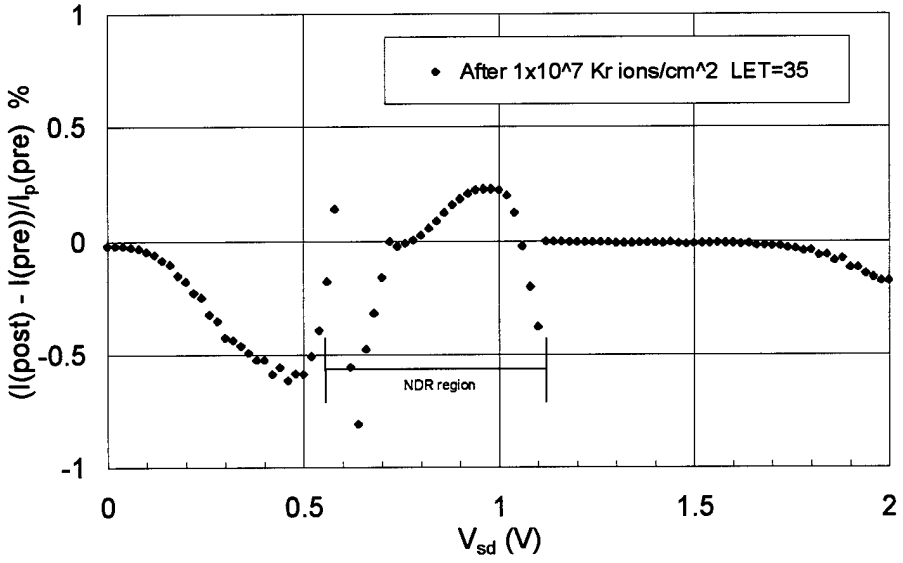

Figure 17. Variation of the post-Kr ion exposure RTD current compared to the pre-radiation current scaled by the RTD peak current I_p.

As was done with the gamma radiation data of Figure 8 (see page 16), a direct comparison of the pre-radiation I-V characteristic with the post-radiation curve was made by subtracting the two curves. The result, shown in Figure 17, was similar to the earlier comparison. The residual curvature was 0.6% at maximum. The difference curve, $\delta I/I_p$ versus V_{sd}, had a shape similar to that produced by a voltage shift of the entire curve, as previously discussed.

RTD Systems Considerations

As previously mentioned, all tests in this report were performed on discrete quantum devices rather than ICs composed of many such devices. While these individual devices exhibited substantial radiation tolerance, the question remained as to their radiation tolerance once connected in large numbers in real circuit applications. One method to address this issue was to compare differences between devices due simply to fabrication with the variations from initial behavior observed after irradiation. This comparison is presented in Figure 18. From this systems point of view, a radiation-hard device should exhibit radiation-induced changes smaller than the differences due to the process variation. Although no systematic radiation effects were

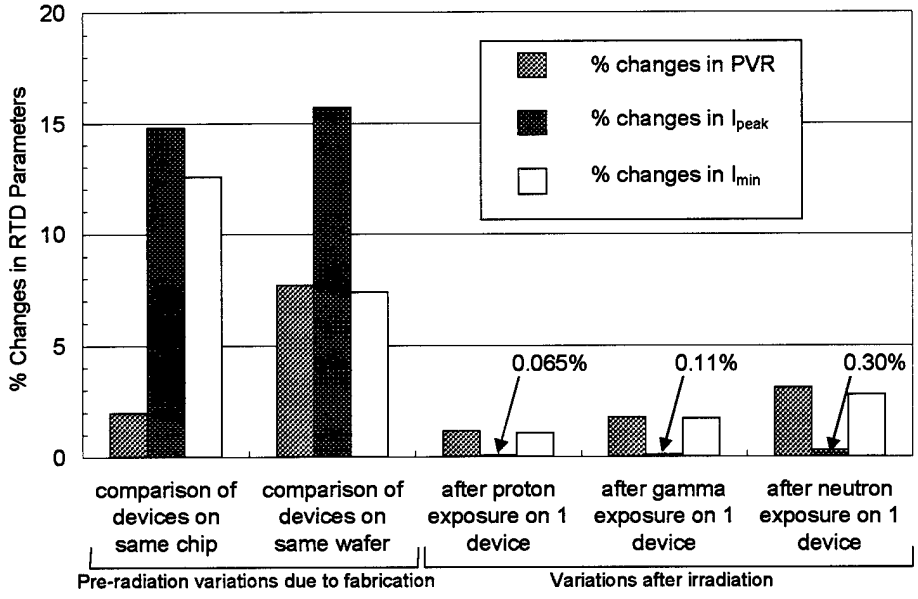

Figure 18. Comparison of fabrication variations for devices located on a single chip and on a single wafer with variations observed in a single device after irradiation.

observed at these fluences, this did limit the magnitude of the radiation effects to be smaller than any measurement variations. As can be seen in the figure, process variation between devices across a wafer and even for devices located on the same chip were considerably larger than the changes observed after irradiation.

One final point from Figure 18 was that for both cases presented the small changes observed in the PVR were almost entirely due to variations in the valley minimum currents. Only small effects were seen in the peak currents at present radiation levels. If these effects were ascribed to irradiation, this might indicate the creation of defects within the barriers that provided non-resonant current paths through the devices.

Two-Dimensional Electron Gas Devices

Pre-Radiation Characterization

For the GaAs/AlGaAs-based 2DEG devices, low temperature magnetotransport measurements were performed to characterize the initial behavior. Under computer control, a current source (Keithley 220) was used with multimeters (HP 3478A) recording the resulting longitudinal and transverse (Hall) voltages. A magnetic field perpendicular to the plane of the epitaxial layers was slowly varied to observe the device behavior. Shown in Figure 19 are data of one such measurement performed at 4.2 K on both the largest area devices and on smaller Hall bars. In the low-field linear region, electron mobilities and carrier densities were extracted from the Hall measurements. In the small area devices, Shubnikov-de Haas oscillations were observed at higher magnetic fields.

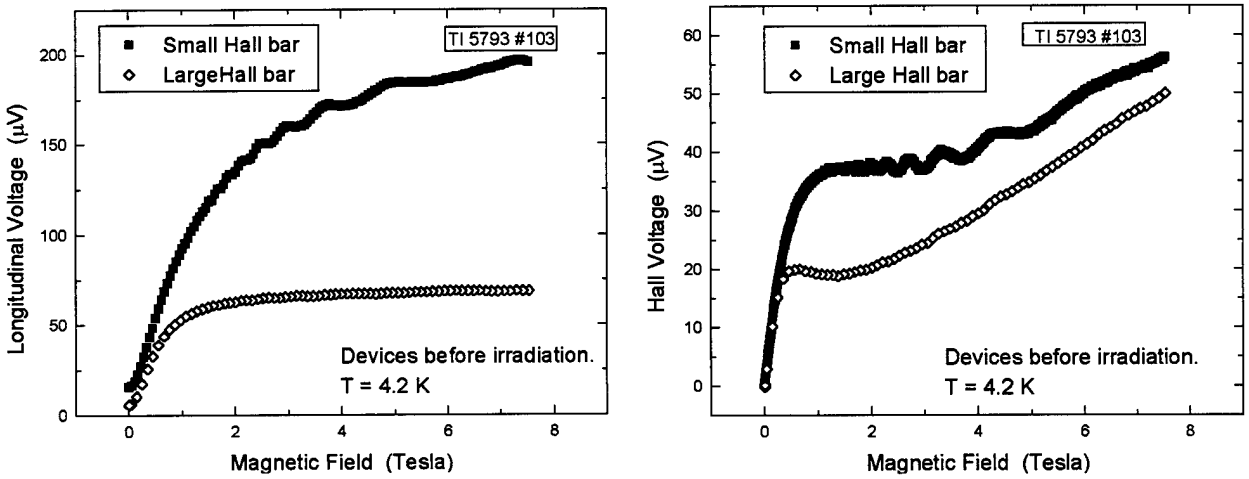

Figure 19. Longitudinal and Hall voltages versus the applied magnetic field for one set of 2DEG devices prior to radiation testing.

The in-plane gated transistors (IPGT) of Figure 2 were characterized by the NanoFAB Center to determine their initial behavior at both room and low temperatures. For a given gate voltage, the source-drain voltage was varied between ±5V starting at 0V and using 50mV steps. Gate voltages were varied between ±3V in 1V steps. An I-V curve for one of the IPGTs at room temperature is shown in Figure 20 and at 4.2 K in Figure 21. Negative gate voltages with respect to the electron conduction channel depleted the devices.

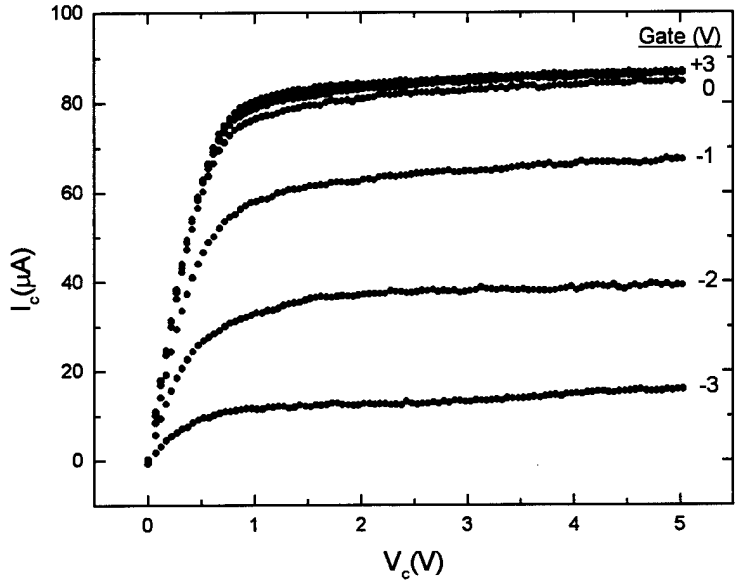

Figure 20. IV curve at room temperature for an in-plane gated 2DEG transistor formed by focused ion beam lithography before any irradiation.

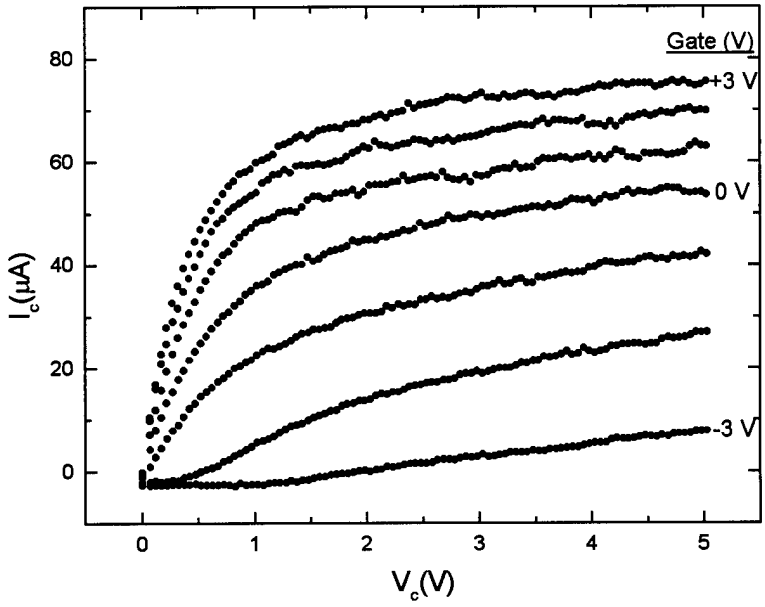

Figure 21. I-V curve for an IPG 2DEG transistor at 4.2 K prior to irradiation.

Gamma Irradiation

Two-dimensional electron gas devices were exposed to gamma radiation from a ^{60}Co source at Texas A&M University. Both large and small 2DEG devices displayed transient effects due to the gamma irradiation. In each case, the channel current through the device was reduced temporarily after gamma irradiation. This current depression was found to relax back toward the initial value over a period of hours after completion of the irradiation.

a. Large-scale 2DEG Hall Bars

The large-area 2DEG devices, built on substrate H039 (see Table 2), received a total of 65 krad of gamma rays at a rate of 234 rad/min. The current through the conduction channel of the devices, I_{sd}, was observed to decrease with continued irradiation. Data from one such experiment, using a device with a channel width of 100 μm, is presented in Figure 22. These large devices were always operated in the linear region of the I-V characteristic. The depression of the current by gamma radiation was expressed by the reduction of the slope of the ohmic I-V as seen in the figure. The total current depression was approximately 5% for this fluence.

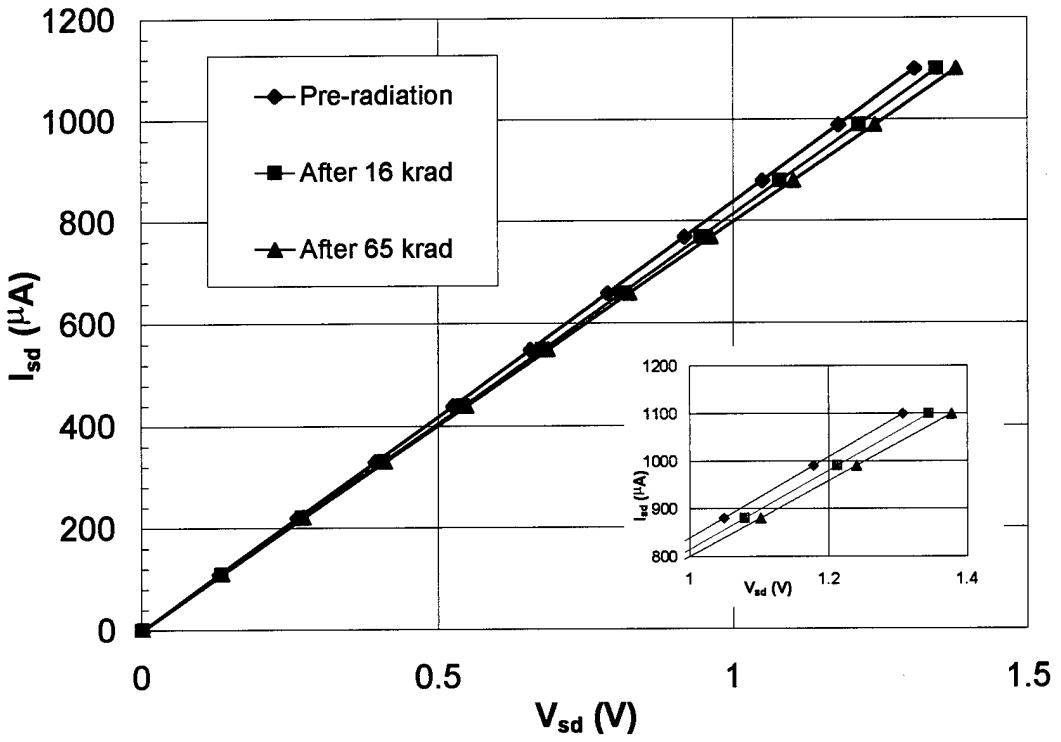

Figure 22. I-V curve for a large 2DEG Hall bar (channel width of 100 μm) at room temperature during gamma irradiation. The radiation depressed the channel current. The inset shows a magnified view of the curve.

For the large 2DEG devices, the onset of the current depression, $(\delta I/\delta V)_{post}/(\delta I/\delta V)_{pre}$, was smooth and the magnitude was a few percent of the initial I-V slope, $(\delta I/\delta V)_{pre}$. This is shown in Figure 23 using data from a 100 μm wide Hall bar. Additionally, the depression appeared to approach a saturation level above roughly 50 krad.

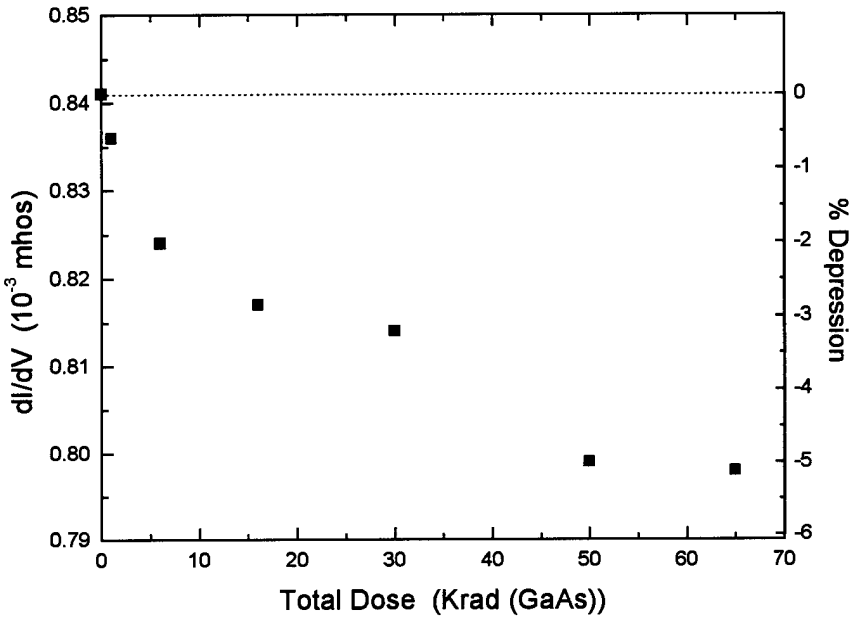

Figure 23. Onset of the current depression with the application of gamma radiation in a large-area 2DEG Hall bar. The absolute change in the slope of the I-V curve is on the left axis; the percent change is on the right axis.

After the gamma exposure ended, the devices were followed to record any subsequent changes at room temperature. The depression was observed to relax back toward the initial, pre-radiation value over a period of hours. An I-V curve depicting the transient recovery of a 100μm Hall bar is shown in Figure 24. A plot of the slope of the I-V curve is shown in Figure 25, giving a better view of the recovery. Over an observation period of 7 hours, this device recovered roughly halfway to the initial value. In this view, the recovery appeared to be composed of fast and slow recovery components. However, the inset of Figure 25 shows a log-log plot of the slope's recovery that is nearly a straight line indicating a power law behavior similar to a diffusion process.

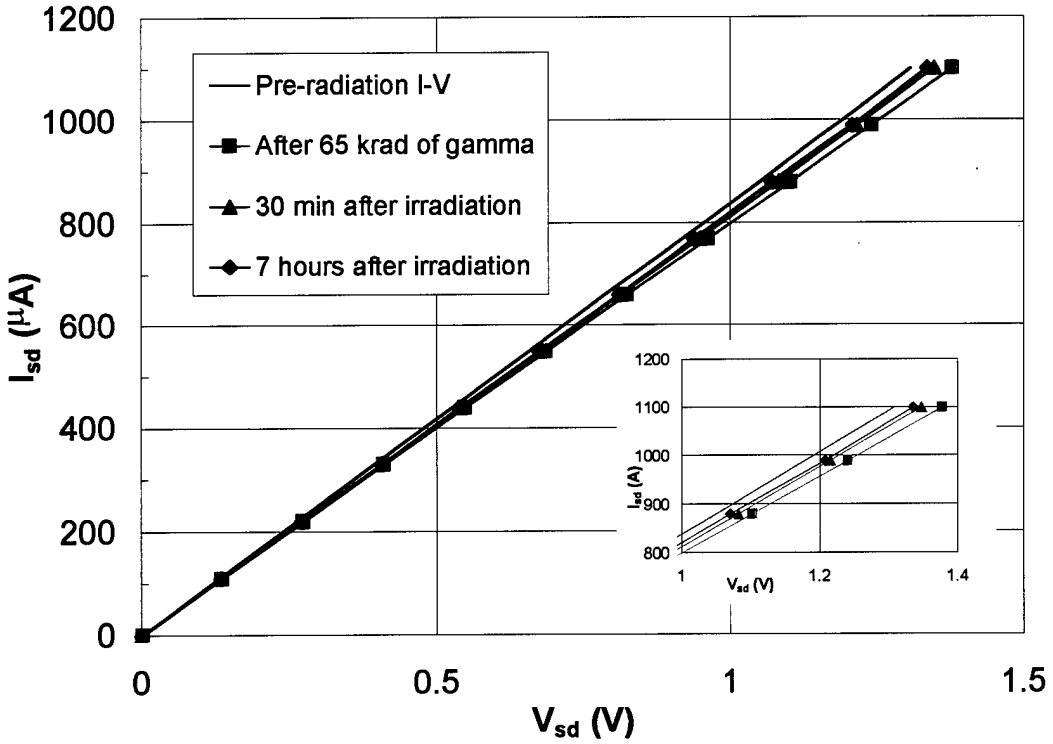

Figure 24. I-V curves showing the recovery of a 100 μm Hall bar after irradiation to 65 krad of ^{60}Co gamma rays. The inset shows a magnified view of one part of the data.

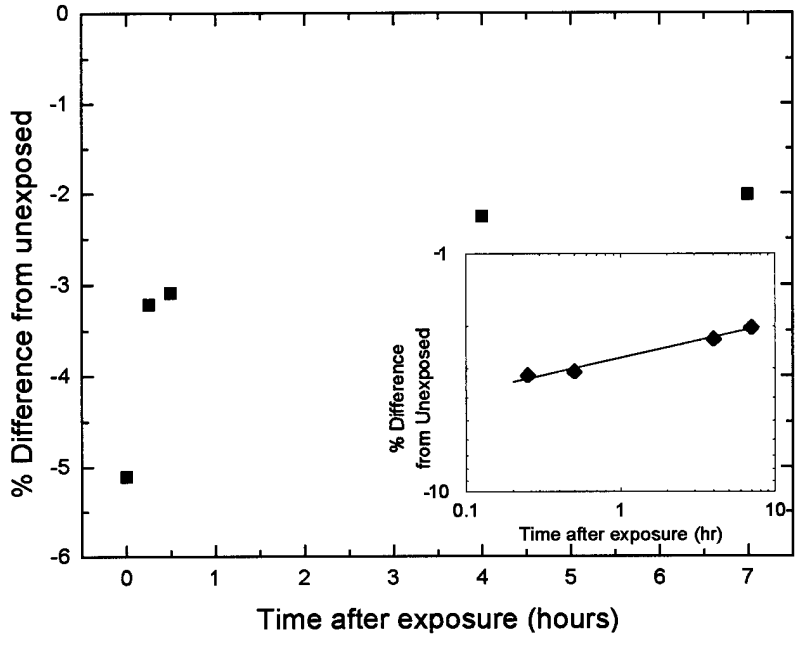

Figure 25. Recovery of the I-V slope of a 100 μm Hall bar after exposure to 65 krad of gamma rays. The inset shows a log-log plot of the recovery with a nearly power law behavior. The straight line is a linear fit to the data.

The behavior of smaller geometry 2DEG devices was the same as the 100 μm Hall bars. Shown in Figure 26 is the I-V curve for a small Hall bar (10 μm channel width) before and immediately after exposure to 65 krad of ^{60}Co gamma rays. This device also displayed a depression of the current proportional to the gamma exposure.

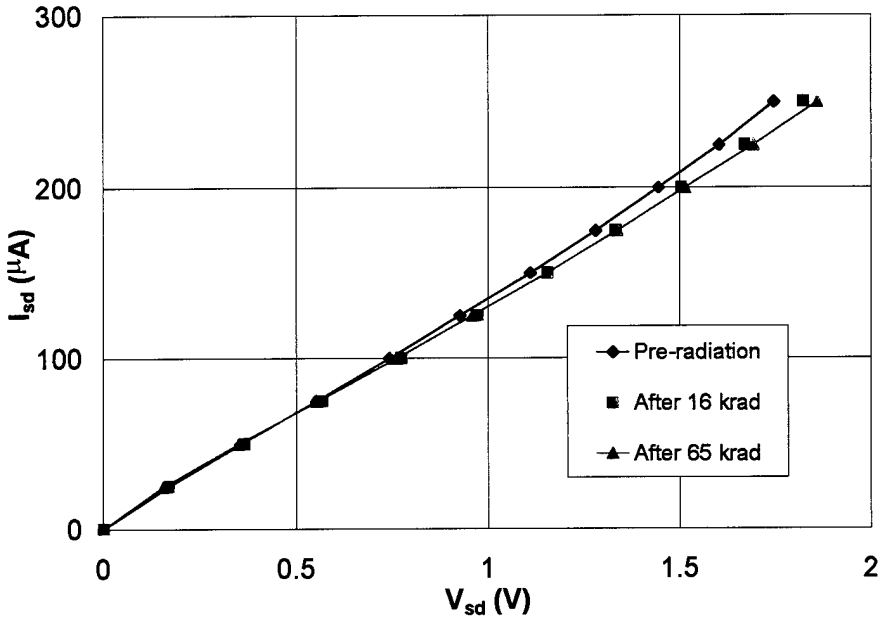

Figure 26. I-V curve of a smaller Hall bar (channel width = 10 μm) before and after exposure to 65 krad of ^{60}Co gamma rays.

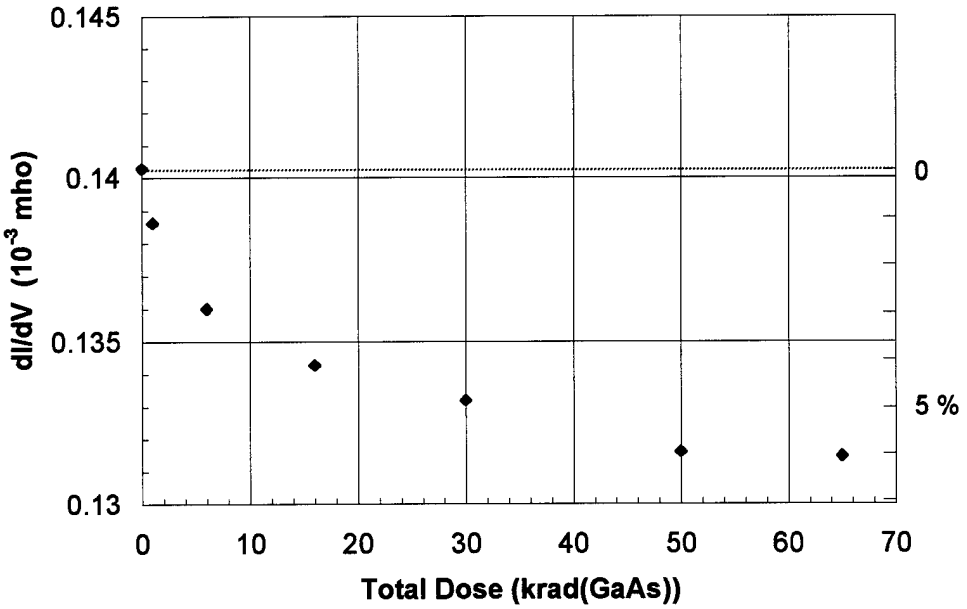

Figure 27. Onset of the current depression with the application of gamma radiation in a 2DEG Hall bar with a channel width of 10 μm.

b. In-plane Gated 2DEG Transistors

The 2DEG in-plane gated transistors (IPGT) were subjected to gamma irradiation using the TAMU ^{60}Co source (Source 'a' of Table 4). Gamma rays were found to reduce the device currents in proportion to the radiation dose. Shown in Figure 28 are I-V curves for an IPGT (substrate RU 9351; see Table 2, page 6) before and after an irradiation to 50 krad at 255 rad/min. This data was taken while the IPGT was being held at a gate voltage of -2V to partially deplete the channel. Immediately after the irradiation, the channel current was found to have been reduced in magnitude. The total depression of the channel current, I_{sd}, was approximately 37% as indicated in the figure. In this manner, the IPGT radiation response was qualitatively the same as that of the 2DEG Hall bars. In each case, gamma irradiation reduced the current through the conduction channel, although the magnitudes were somewhat different. Also shown in this figure is an I-V curve taken 4 hours after completion of the irradiation. By this time, the device had recovered almost completely to its pre-radiation characteristic.

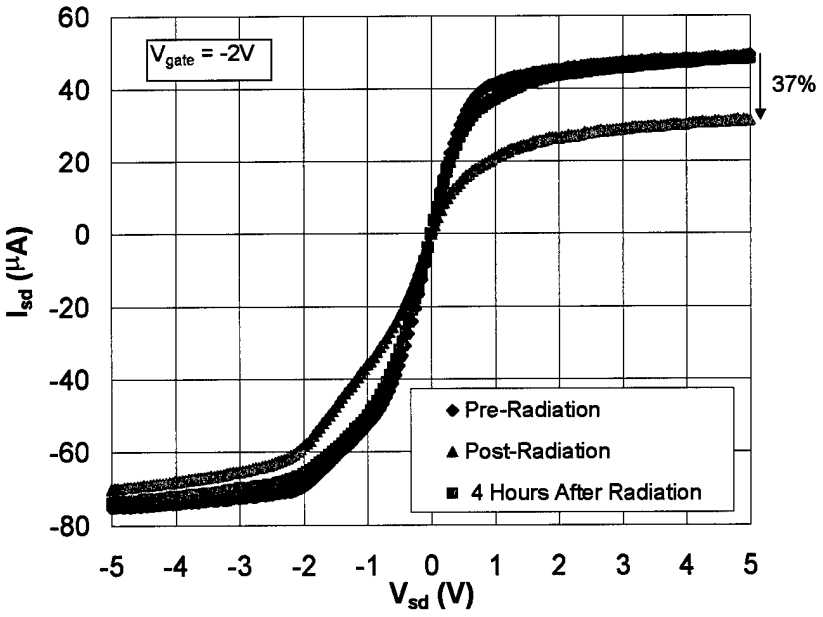

Figure 28. I-V behavior of a 2DEG IPGT before and after exposure to 50 krad of ^{60}Co gamma rays at a rate of 255 rad/min. The irradiation depressed the device current by 37% after completion. The current recovered nearly completely over a period of 4 hours.

The onset of the IPGT current depression for this substrate (RU9351) with gamma dose is plotted in Figure 29. The device response appeared to approach a saturation level at the upper end of the exposure. The data is reasonably fit by an exponential decay with a characteristic dose of 10.87 krad(GaAs). No systematic dose rate studies were performed on these devices.

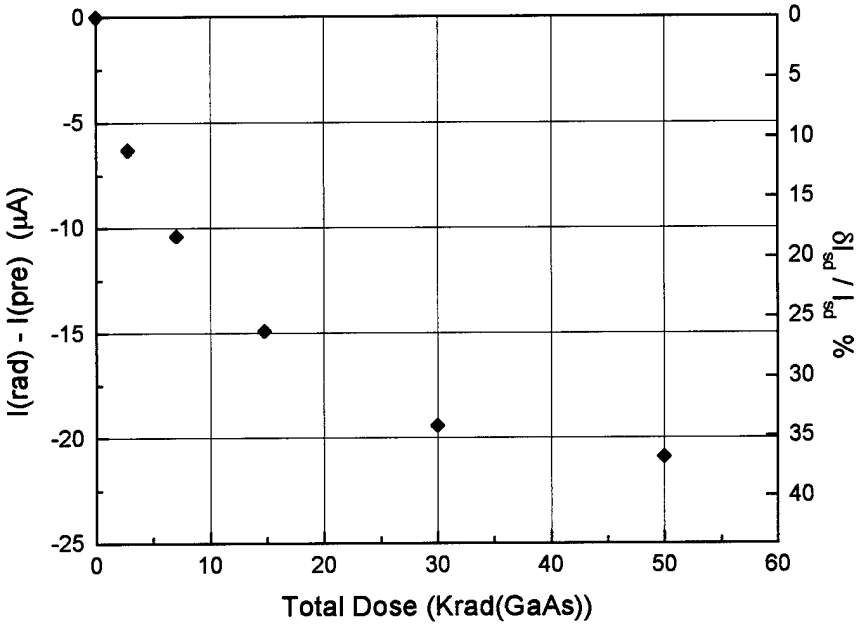

Figure 29. Onset of channel current depression in an IPGT (substrate RU 9351) during gamma irradiation to 50 krad at 255 rad/min.

These devices also displayed a smooth recovery after the radiation stopped. This is shown in Figure 30.

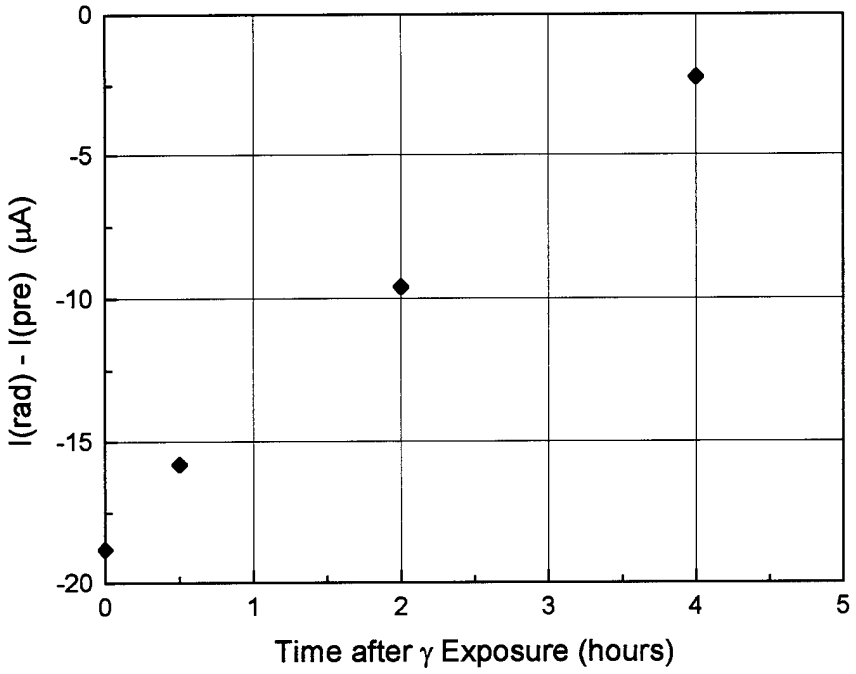

Figure 30. Recovery of IPGT (substrate RU 9351) following irradiation to 50 krad of gamma rays.

Proton Irradiation

The 2-DEG transistors also underwent proton tests (55 MeV protons) to a total fluence of 5×10^{10} protons/cm^2. Typical results of these tests for a device on the substrate RU 9351 are presented in Figure 31. For a given gate voltage (-3V in this case), the device channel currents increased under energetic proton irradiation. This "positive" current shift was about 39% for this device, or the same order of magnitude as the "negative" current shift observed for the gamma irradiation. Other devices from this substrate were irradiated and displayed the same current enhancement, although the magnitude varied from one device to another. This variation is seen in Figure 32, which records the appearance of a current enhancement of 62%, with a proton fluence to 5×10^{10} protons/cm^2. Also, the magnitude of the shift was proportional to the proton flux. Initially the devices were irradiated to 5×10^{9} protons/cm^2 and a current shift was observed followed by slow recovery toward the initial IV characteristic. Subsequent irradiation up to a total fluence of 5×10^{10} protons/cm^2 increased the current shift. The devices did not fully recover their pre-radiation characteristics under observation of up to four hours after irradiation.

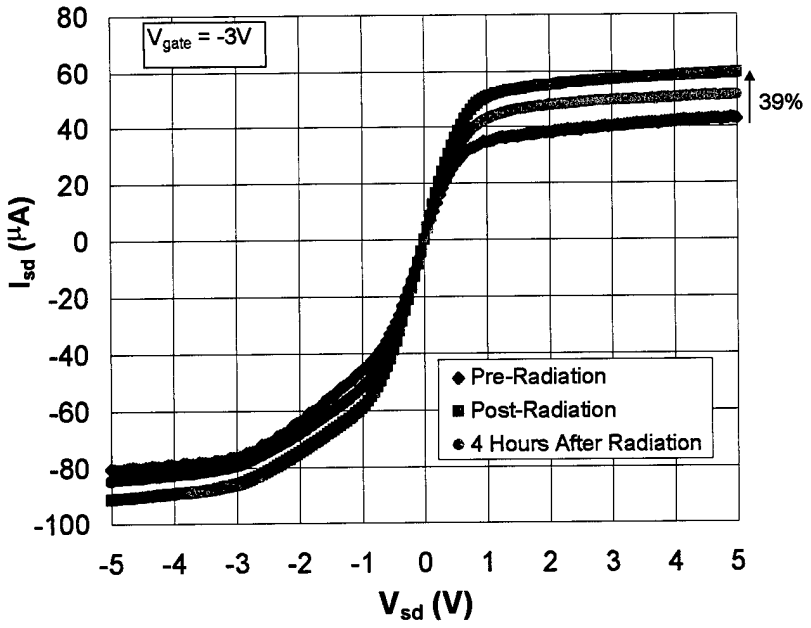

Figure 31. I-V behavior of a 2DEG IPGT (substrate RU 9351, IPGT #1) before and after exposure to 5×10^{10} protons(55MeV)/cm^2. During the irradiation, V_{gate} = -3V. The radiation caused an enhancement of the channel current through the device of about 39%.

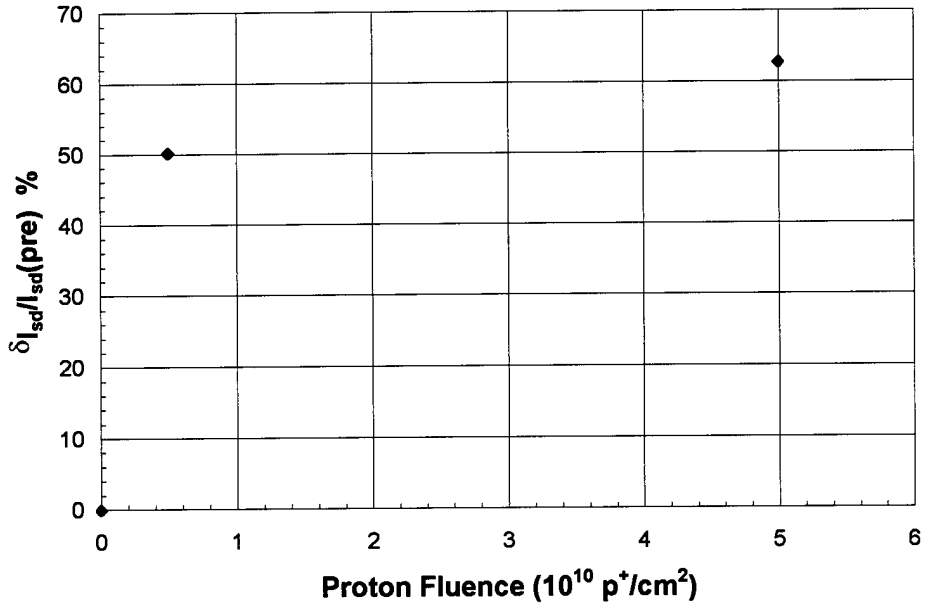

Figure 32. Onset of channel current enhancement with proton exposure in a different 2DEG IPGT (substrate RU 9351, IPGT #5). This IPGT underwent a larger current enhancement than the one depicted in Fig 31, amounting to ~62%.

Further proton irradiation tests were performed on 2DEG IPGTs that were constructed on a different epitaxial substrate (RU 1216; see Table 2 on page 6). These two substrates had similar, though not identical, epitaxial film parameters and electrical characteristics. The beam characteristics were identical to the initial proton tests: 55 MeV protons at a flux of 5×10^7 protons/cm^2-sec to a total fluence of 5×10^{10} protons/cm^2. These devices displayed the same effects as in the earlier experiments: exposure to protons caused a transient enhancement of the IPGT channel current. However, the magnitude of the effect was significantly smaller. This is shown in Figure 33, in which the size of $\delta I_{sd}/I_{sd}$ was only ~6.5%. The current enhancement is shown magnified in the inset of the figure.

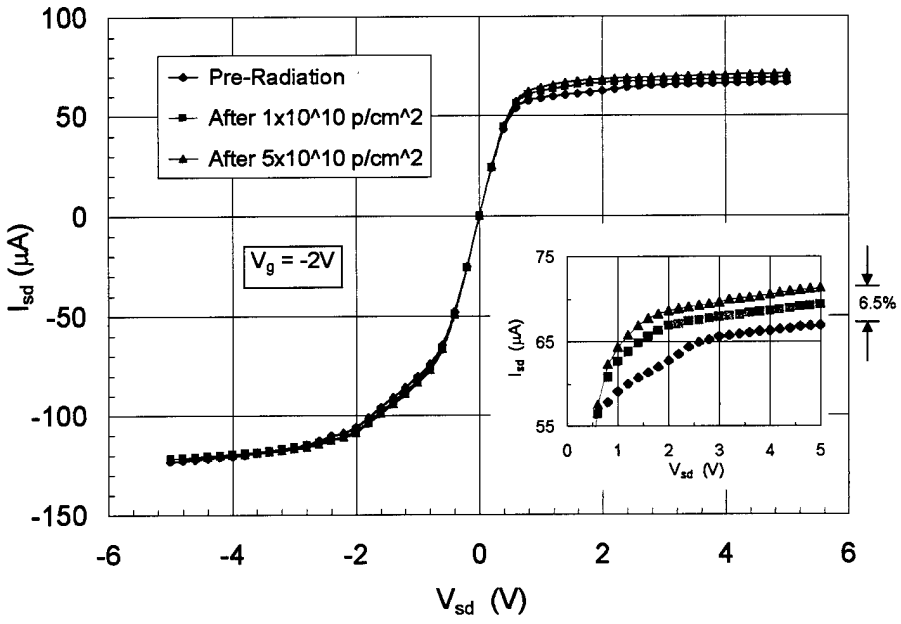

Figure 33. I-V curves for an IPGT on the substrate RU 1216 from pre-radiation through the total fluence of 5×10^{10} protons/cm^2. The proton exposure of these devices also caused an enhancement of the channel current although the size of the effect was much smaller than the initial tests on substrate RU 9351. The enhancement is shown magnified in the inset of the figure.

As can be seen in Table 2, there are some differences between the two substrates both physically and in their electrical characteristics. The earlier substrate, RU 9351, had a larger low-temperature mobility despite its smaller AlGaAs spacer layer and higher two-dimensional carrier density. The lower quality of the second substrate, RU 1216, might have rendered its devices less susceptible to radiation effects. Further studies with several different substrates would be necessary to determine this.

Another way to see the current enhancement turn-on is shown in Figure 34. This figure displays a plot of the channel current, I_{sd}, versus the applied gate voltage, V_g, at a fixed voltage bias of $V_{sd} = +3V$. The greatest relative effect was seen at high values of V_g. The development of the current enhancement with proton exposure may be seen more clearly in Figure 35.

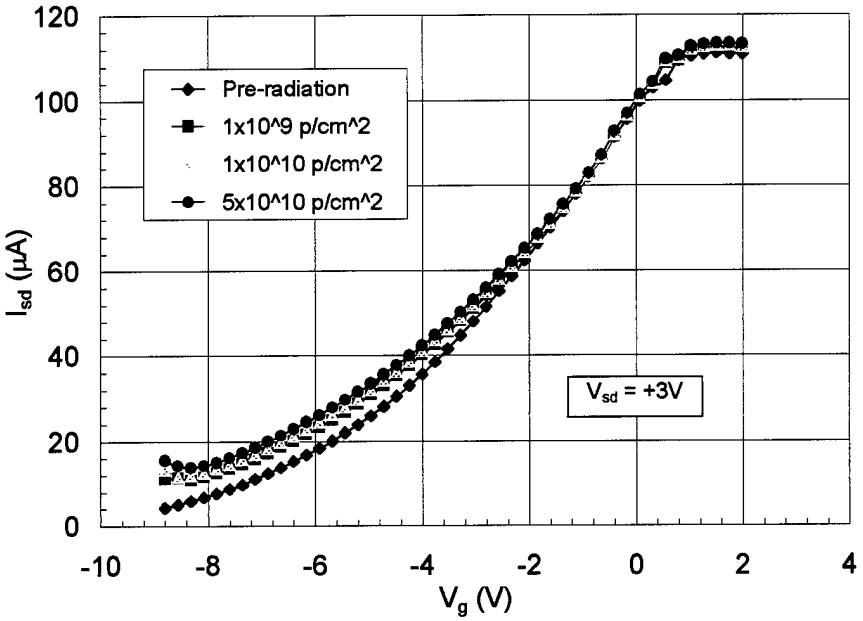

Figure 34. Plot of the channel current versus gate voltage showing the appearance of the current enhancement with proton exposure for an IPGT from the later substrate RU 1216.

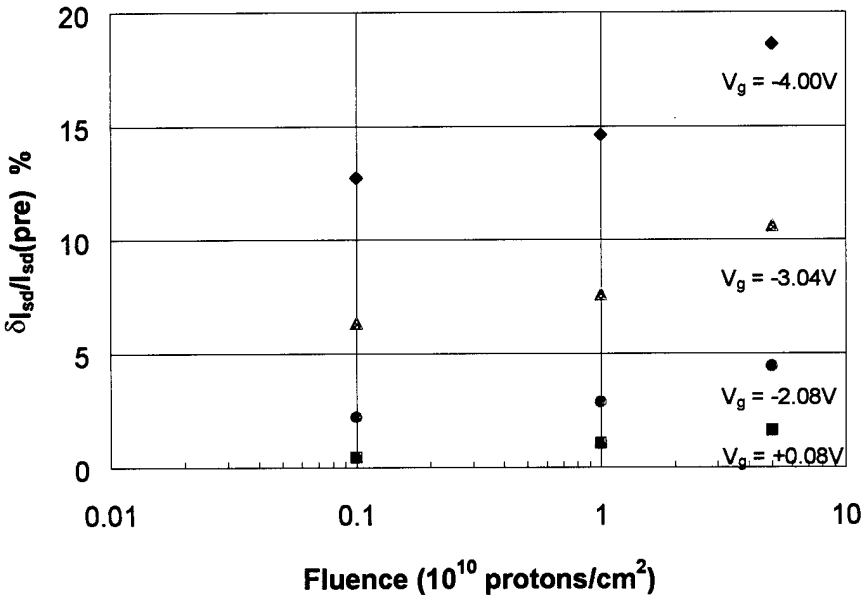

Figure 35. Log-linear plot of the onset of the current enhancement in an IPGT from RU 1216 during proton exposure at various gate voltages while at $V_{sd} = +3V$.

In this latter radiation test, data was taken to look for changes in device operation as indicated through the transconductance, $g_m = \delta I_{sd}/\delta V_g$. One such data set is shown in Figure 36 taken from the same IPGT as in Figure 33. The only noticeable difference between the curves was the depression of the irradiated g_m compared to the pre-radiation g_m in the range of $V_g \sim -2V$ to -4V.

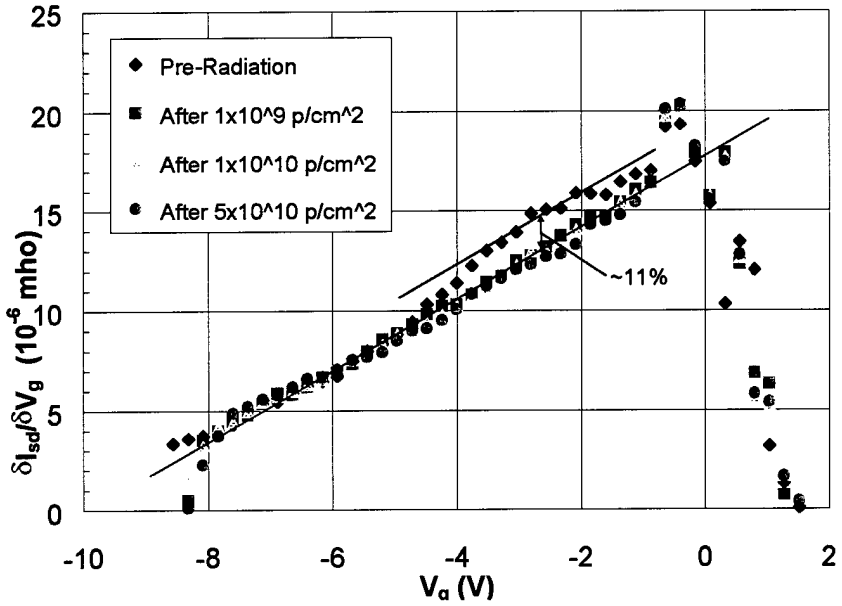

Figure 36. Plot of the transconductance of an IPGT from RU 1216 versus V_g during its exposure to 55 MeV protons.

Finally, the proton-induced current enhancement in the IPGTs also was found to be a transient effect. These devices were followed for a period of two hours after the end of the proton exposure. In that time period, the devices typically recovered about halfway back to their original, pre-radiation I_{sd} levels. This is shown in Figure 37. This transient recovery is the same as that observed for the original devices on substrate RU 9351. The same recovery is shown in Figure 38 for several values of gate voltage, V_g.

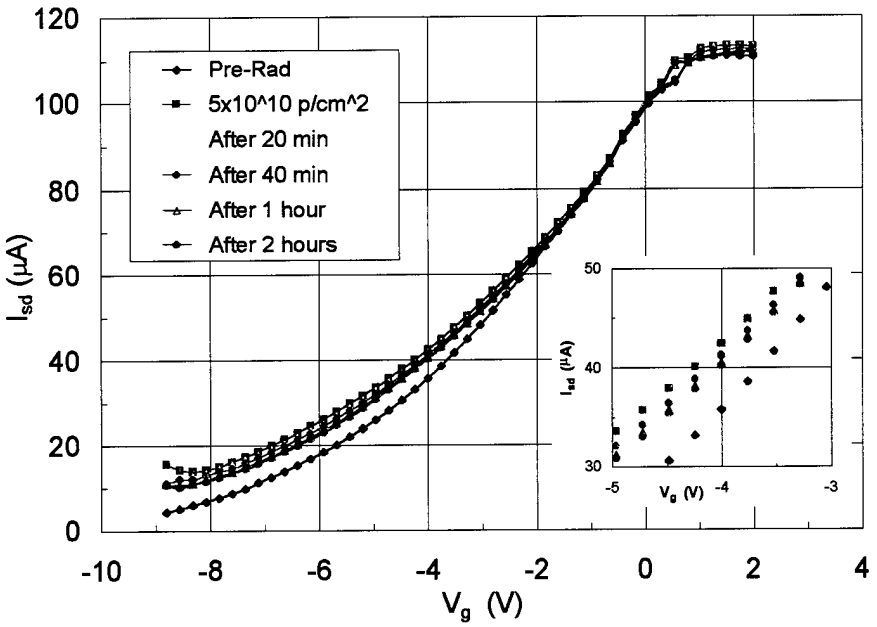

Figure 37. Plot showing the recovery of the proton-induced current enhancement for two hours following the completion of the irradiation. The current recovered about halfway back to its original value in this time. The inset shows a magnified view of the range from V_g = -3 to -5V.

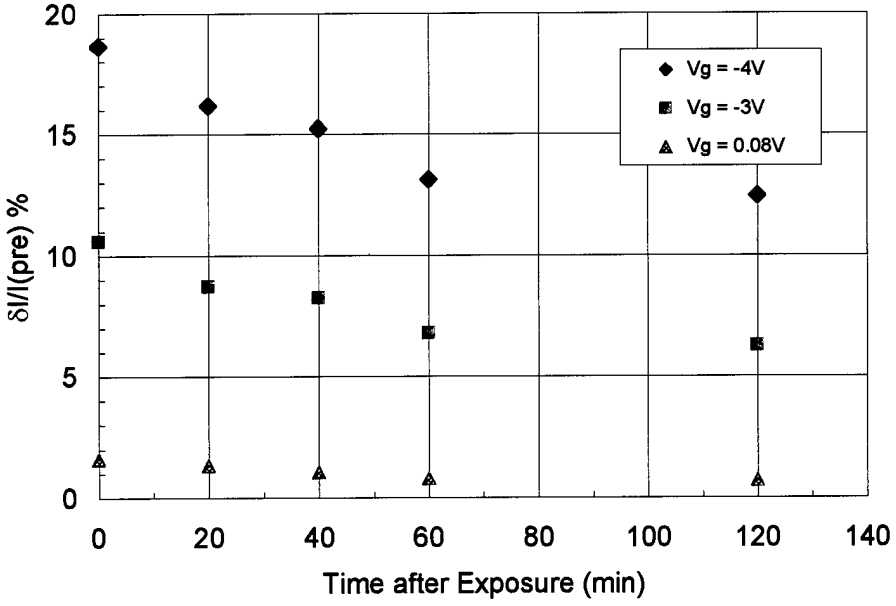

Figure 38. Plot showing the recovery of an IPGT from substrate RU 1216 after exposure to 5×10^{10} protons/cm^2 at 55 MeV. The recovery is shown at several different values of gate voltage.

Neutron Irradiation

Some of the 2DEG IPGTs from substrate RU 9351 were exposed to energetic neutron irradiation at the Los Alamos Neutron Science Center. The total fluence these devices experienced was 3×10^{10} neutrons/cm^2 with energies ranging from 1–800 MeV. In this case, the IPGTs did not display any significant changes, transient or otherwise, due to the exposure. Results of these tests for one device are shown in Figure 39. This figure presents the I_{sd}-V_{sd} characteristics for pre- and post-radiation curves. To check for changes in device operation, data was also taken for I_{sd}-V_g. This is presented in Figure 40. This result may indicate the importance of electric charge in the transient effects seen with other radiation species. In the proton effect, the proton's charge might enhance the expected atomic displacement to observable levels compared with the neutron; in the case of the gamma transient, it's ionizing effect along it's path may directly deplete the conduction channel for some time before the excess charge leaks out.

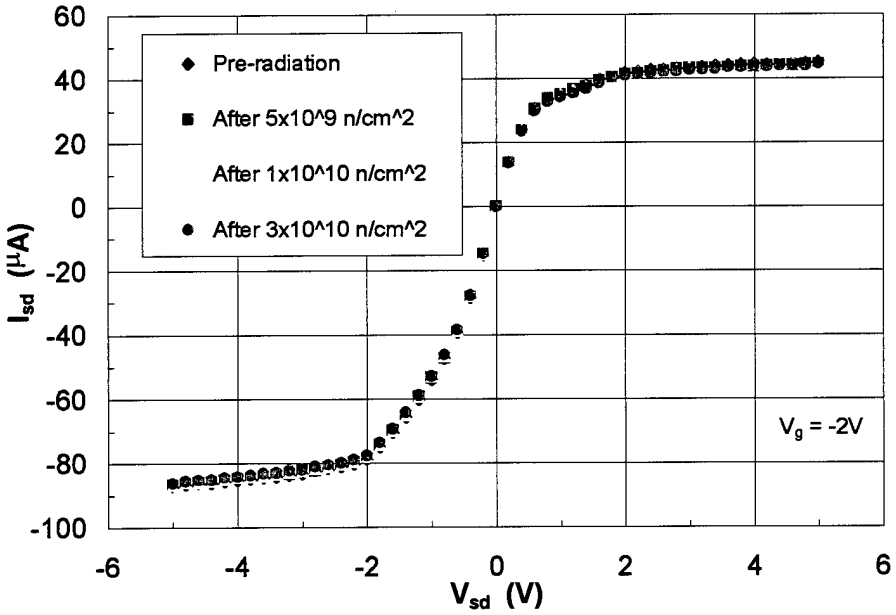

Figure 39. Plot of the I_{sd}-V_{sd} curve for an IPGT from RU 9351 before and after irradiation by energetic neutrons to a fluence of 3×10^{10} neutrons/cm^2. No effect of the irradiation was seen.

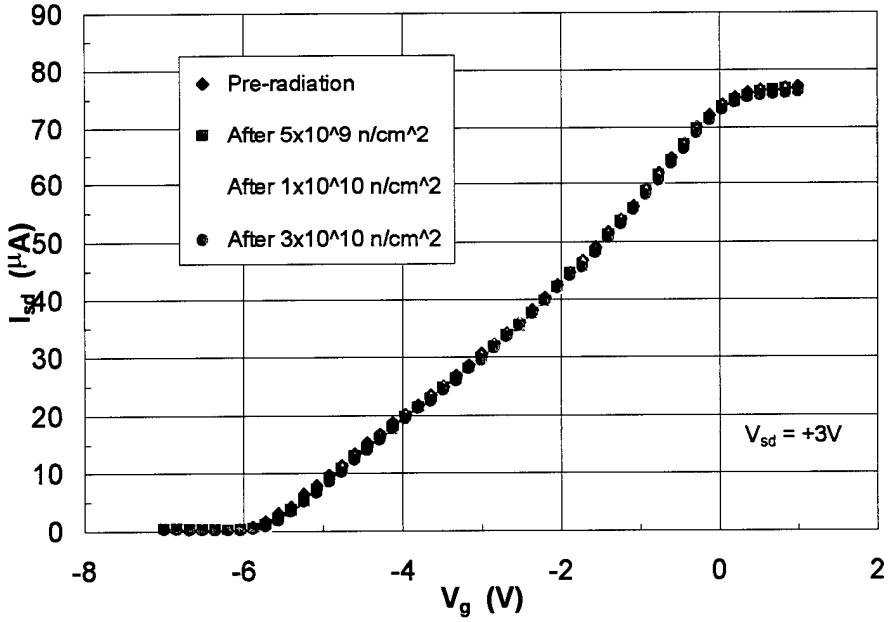

Figure 40. Plot of I_{sd} versus V_g for the same IPGT from RU 9351 before and after neutron irradiation, again showing no effects of the radiation on device operation.

Personnel Supported

UTA NanoFAB Center:

1. **W. P. Kirk**, (Director, NanoFAB): Overall project management. Organize and design device fabrication. Arrange donation of devices from other research groups. Monitor project progress, conduct meetings and briefings on critical path items.
2. **R. T. Bate**, (senior research scientist): Provided liaison with Raytheon TI Systems, plan reviews, provide advice on device characterization results and assist with reports.
3. **G. F. Spencer**, (research scientist): Installed processing equipment in cleanroom, design devices and circuits, device fabrication, coordinate effort with PVAMU, write reports.
4. **J. Ryan**, (postdoctoral researcher): Set up device processing lab components in cleanroom.
5. **R. Klima**, (research instrumentation specialist): Provide equipment setup and maintenance.
6. **D. Smith**, (technician): Provide technical equipment setup and maintenance.
7. **J. Florence** (technician): Provide technical equipment setup and maintenance.
8. **A. Wolven**, (technician): Provide technical equipment setup and maintenance.
9. **E. Maldonado**, (graduate student/research associate): Epitaxial growth of III-V materials for 2DEGs and RTDs.
10. **H. Jiang**, (graduate student): Device measurement over full temperature ranges.
11. **K. Clark**, (graduate student): Cryogenic device characterization to establish baseline for RTD structures. Instruct PVAMU personnel on handling and measuring techniques for RTD structures. Assist with MBE growth.
12. **T. Zhou**, (graduate student): MBE growth of 2DEG and RTD structures.
13. **J. Morris** (undergraduate student): General assistance with project.
14. **A. Ali** (undergraduate student): General assistance with project.
15. **D. Finster** (undergraduate student): General assistance with project and computer network.
16. **M. Perdue** (undergraduate student): General assistance with project and equipment repair.
17. **L. Bourree** (undergraduate student): General assistance with project and equipment repair.

PVAMU CARR:

1. **T. N. Fogarty** (Director, CARR): Conducted and supervised radiation tests; monitored project progress; evaluation of data.
2. **R. Wilkins** (Deputy Director, CARR): Conducted and supervised I-V measurements, radiation tests and data interpretation, presented poster and talks, secured beamtime on Los Alamos neutron source, prepared publications.
3. **A. Kumar** (CARR faculty): Conduct and supervise literature search; evaluate commercially available simulation software.
4. **D. Wu** (research scientist): Modeling of device characteristics and effects.
5. **J. Gryko** (research scientist): Modeling of device characteristics and interpretation of data.
6. **S. Shojah-Ardalan** (research engineer): Prepared apparatus for radiation tests, conducted radiation tests, collected and processed data; evaluated data; development of data handling procedures, prepared test reports.
7. **S. Shokrzadeh** (graduate student): Fabricated test apparatus.
8. **A. Caceres** (graduate student): Conduct literature search.
9. **E. Jackson** (undergraduate student): Assist with radiation tests.

Publications Resulting from this Project

1. *Nonparabolicity effects in the bipolar quantum-well resonant-tunneling transistor*, K. P. Clark, W. P. Kirk, and A. C. Seabaugh, Phys. Rev. B 55, 7068 (1997).
2. *Radiation Effects on Resonant Tunneling Diodes: Preliminary Results*, R. Wilkins, S. Ardalan, E. Jackson, and J. Gryko, NASA University Research Centers Series Vol. II (TSI Press, Albuquerque, NM, 1998) pg.125.
3. *Studies of Radiation Effects in Quantum Devices*, W. P. Kirk, R. T. Bate, G. F. Spencer, R. Wilkins, S. Ardalan, and T. Fogarty, Proceedings of NanoSpace 98, 1998.
4. *Ionization and Displacement Damage Irradiation Studies of Quantum Devices: Resonant Tunneling Diodes and Two-Dimensional Electron Gas Transistors*, R. Wilkins, S.S. Ardalan, W.P. Kirk, G.F. Spencer, R.T. Bate, A.C. Seabaugh, R. Lake, P. Stelmaszyk, and A.D. Wieck and T.N. Fogarty, IEEE Trans. Nuc. 46, 1702 (Dec 1999).
5. *Radiation Effects in Discrete Quantum Devices*, G. F. Spencer, W. P. Kirk, R. T. Bate, R. Wilkins, S. S. Ardalan, T. N. Fogarty, A. C. Seabaugh, P. Stelmaszyk, and A. D. Wieck, Gov. Microcir. Appl. Conf. Digest of Papers, vol XXV, 351 (March 2000).

Interactions and Transitions

W. P. Kirk, **R. T. Bate**, and **G. F. Spencer** traveled to the AFOSR Program Review in Dayton, Ohio on September 29, 1999. A talk was presented by Spencer at this meeting, reviewing the status and plans for the current research program. Discussions were held with AFOSR representatives regarding the next phase of this research program. A white paper describing this proposed work was submitted to them. **Spencer** also traveled to the 25th Government Microcircuit Applications Conference, which was held 20-23 March 2000 in Anaheim, California, to present a talk on the results of this research program. Discussions were held with representatives of the Defense Threat Reduction Agency (including **A. Costantine**) regarding their interest in supporting the next phase of this research. A revised white paper and proposed budget have been submitted for their consideration.

Presentations at Professional Meetings

1. *Radiation Effects on Resonant Tunneling Diodes*, R. Wilkins, J. Greco, S. Ardalan, and E. Jackson, National Alliance of NASA URCC (Feb. 1998).

2. *Radiation Effects in Quantum Devices*, W. P. Kirk, NanoSpace 98: International Conference on Integrated Nano/Microtechnology for Space Applications, Houston, TX, invited talk (November, 1998).
3. *Proton and Gamma Irradiation on InP-based Resonant Tunneling Diodes*, R. Wilkins, B.D. Weaver, S. Shojah-Ardalan, W.P. Kirk, G.F. Spencer, R.T. Bate, A.C. Seabaugh, R. Lake, and T.N. Fogarty, poster presented at the 1999 NASA/JPL Conference on Electronics for Extreme Environments, available at http://extremeelectronics.jpl.nasa.gov/conference.
4. *Radiation Effects on Quantum Devices*, R. Wilkins, invited talk, Air Force Research Laboratory, Kirtland Air Force Base, New Mexico, July 2, 1999.
5. *Ionization and Displacement Damage Irradiation Studies of Quantum Devices: Resonant Tunneling Diodes and Two-Dimensional Electron Gas Transistors*, R. Wilkins, 1999 Nuclear and Space Radiation Effects Conference, Norfolk, VA, contributed talk (15 July 1999).
6. *Radiation Effects in Discrete Quantum Devices*, G. F. Spencer, AFOSR Contractors' Review Meeting, Dayton, OH (September 29, 1999).
7. *Radiation Studies of Quantum Devices*, R. Wilkins, LANSCE User's Group Meeting, Los Alamos Neutron Science Center, Los Alamos, NM (February, 2000).
8. *Radiation Effects in Quantum Devices*, G. F. Spencer, Government Microcircuit Applications Conference 2000, Anaheim, CA (March 23, 2000).
9. *Radiation Tolerance of Discrete Quantum Devices*, G. F. Spencer, poster presented at the Spring Poster Festival of the Metroplex Research Consortium for Electronic Devices and Materials, University of North Texas, Denton, TX (March 30, 2000).

New Discoveries, Inventions, or Patent Disclosures

None

Honors and Awards

None

Student Theses Based on this Project (in whole or part)

S. S. Ardalan, Master's project for M.S., Prairie View A&M University
"Total dose radiation study on the electrical characterization of resonant tunneling diodes"

[1] See, for example: "Quantum Devices & Applications", *Proc. IEEE* **87**, (April, 1999).
[2] S-J. Wei, H. C. Lin, R. C. Potter, and D. Shupe, *IEEE J. Solid-State Cir.* **28**, 697 (1993).
[3] J. I. Bergman, J. Chang, Y. Joo, B. Matinpour, J. Laskar, N. M. Jokerst, M. A. Brooke, B. Brar, and E. Beam III, *IEEE Elect. Dev. Lett.* **20**, 119 (1999).
[4] S. L. Rommel, T. E. Dillon, P. R. Berger, R. Lake, P. E. Thompson, K. D. Hobart, A. C. Seabaugh, and D. S. Simons, *Int. Elect. Dev. Meeting Tech. Dig. (IEDM 98)*, 1035 (1998).
[5] R. Bouregba, O. Vanbésien, P. Mounaix, D. Lippens, L. Palmateer, J. C. Pernot, G. Beaudin, P. Encrenaz, E. Bockenhoff, J. Nagle, P. Bois, F. Chevoir, and B. Vinter, *IEEE Trans. Micro. Theory and Tech.* **41**, 2025 (1993).
[6] P. D. Buckle, P. Dawson, M. A. Lynch, C-Y. Kuo, M. Missous, and W. S. Truscott, *Proc. IEEE 6th Int. Conf. on THz Electr.I,* 82 (1998).
[7] E. M. Jackson, B. D. Weaver, A. C. Seabaugh, J. P. A. Van der Wagt, and E. A. Beam III, *Appl. Phys. Lett.* **75**, 280 (1999).
[8] V. J. Goldman, D. C. Tsui, and J. E. Cunningham, "Observation of intrinsic bistability in resonant-tunneling structures", Phys. Rev. Lett. **58**, 1256 (1987).
[9] L. E. Eaves, F. W. Sheard, and G. A. Toombs, in *Physics of Quantum Electron Devices*, edited by F. Capasso, (Springer, Berlin, 1990) p. 136.